NASA TECHNICAL MEMORANDUM

NASA TM X-1521

C. 2



# FLIGHT INVESTIGATION AND ANALYSIS OF ALLEVIATION OF COMMUNICATIONS BLACKOUT BY WATER INJECTION DURING GEMINI 3 REENTRY

*by Lyle C. Schroeder and Francis P. Russo*

*Langley Research Center*
*Langley Station, Hampton, Va.*



NATIONAL AERONAUTICS AND SPACE ADMINISTRATION • WASHINGTON, D. C. • MARCH 1968

NASA TM X-1521



# FLIGHT INVESTIGATION AND ANALYSIS OF ALLEVIATION OF COMMUNICATIONS BLACKOUT BY WATER INJECTION DURING GEMINI 3 REENTRY

By Lyle C. Schroeder and Francis P. Russo

Langley Research Center
Langley Station, Hampton, Va.



NATIONAL AERONAUTICS AND SPACE ADMINISTRATION

# FLIGHT INVESTIGATION AND ANALYSIS OF ALLEVIATION OF COMMUNICATIONS BLACKOUT BY WATER INJECTION DURING GEMINI 3 REENTRY*

By Lyle C. Schroeder and Francis P. Russo
Langley Research Center

## SUMMARY

A method of overcoming reentry communications blackout by injecting water into the flow field was demonstrated during the Gemini-Titan 3 (GT-3) mission. Significant levels of signal-strength increase during the early portion of the water injection sequence over an altitude range from 272 000 to 246 000 ft (82.90 to 74.98 km) were noted by ground stations on VHF telemetry (230.4 MHz) and VHF voice (296.8 MHz). Enhancement of C-band beacon signal (5690 MHz) was observed during the latter portion of the water injection sequence over an altitude range from 200 000 to 160 000 ft (60.96 to 48.77 km).

VHF signal recovered during water injection at various ground stations indicated that the antenna pattern was directed in the radial direction of injection from the spacecraft, in agreement with preflight predictions.

Previous work has shown that the most probable cause of the loss of VHF signal recovered is reduced injectant penetration, although nonoptimum antenna location, injection site, vehicle attitude, and insufficient persistance of the communications window may have been principal factors.

A comparison of calculated electron concentration, based on theory in which recombinations at or near the surface of water drops are assumed to be the primary mechanism of causing reduction of the electron concentration, with values deduced from the observed VHF attenuation data is reviewed.

The C-band signal attenuation during the Gemini 3 reentry was not predicted. The C-band attenuation and recovery are explained on the basis of ablation products in the separated-flow plasma.

---

*Title, Unclassified.

## INTRODUCTION

Reentering manned spacecraft usually suffer a lapse in communications, or a communications blackout, due to interaction of electromagnetic energy with free electrons thermally generated in the oblique bow shock. Blackout has averaged about 5 minutes on Mercury and Gemini and is expected to last much longer on Apollo spacecraft earth reentry from lunar missions. Because tracking during reentry is important in determining the landing point of the spacecraft and this period presents the most severe heating, acceleration, and guidance problems for the spacecraft, it is desirable to restore communications during all or part of the blackout.

Methods of alleviating communications blackout have been sought for some time. Various techniques studied as a part of Project RAM (Radio Attenuation Measurement) have included use of static magnetic fields, aerodynamic shaping, microwave carrier signals, and material injection into the flow field. Each of these studies culminated in a flight test of the respective alleviation technique on a slender probe (refs. 1 to 3).

One of the most significant results of these flight tests was the almost complete elimination of radio attenuation by the injection of water into the plasma sheath from the stagnation point and from sites on the sides of the RAM B2 (ref. 3). The signal recovery due to side injection is of particular significance to the Gemini or Apollo spacecraft because it showed that water injection does not have to encompass the entire flow field to be effective but can be confined to the flow field in the vicinity of the antenna.

To test the window concept further on large blunt spacecraft, an in-flight water injection experiment was conducted during the reentry of the Gemini 3 spacecraft on March 23, 1965. Recovery of both the VHF and C-band (which was not expected to be attenuated) signals was noticed during parts of the attenuation period; this demonstrated that blackout alleviation by creating a window in the plasma sheath of large blunt-nose spacecraft is feasible. These results were previously reported in references 4 to 6.

This report presents (1) the experiment concept, (2) review of studies made to determine how to achieve the proper size window, (3) the Gemini 3 results, and (4) an analysis of the signal-strength results in light of the design parameters, the predicted flow-field electron concentration, and the predicted radiation patterns. In the appendix by Francis P. Russo and Aubrey E. Cross is discussed an experimental simulation of the VHF radiation pattern of the Gemini spacecraft surrounded by a plasma sheath with a communications window. Frequent use is made of the work reported in reference 7 for water injection parameters and initial design estimates of water flow rate, in reference 8 for analysis of the flight results from a fluid mechanics standpoint and for theoretical calculations of electron concentration $N_e$ and comparison with the data, and in references 9 and 10 for the analysis of C-band signal recovery.

## EXPERIMENT DESIGN

### Experiment Concept

The concept of this experiment was to create a signal transmission window in the plasma sheath by the injection of water into a narrow slice of the flow field from the side of a large blunt body. Although mass flow requirements for the whole flow field of a blunt body are quite large, the mass flow requirements can be considerably reduced if injection is confined to a narrow slice or sector of the flow field. Therefore, the first step in the design was to determine a minimum window size which would result in restoration of the signal.

It was required that the electron concentration be reduced below the critical level for VHF signal transmission ($N_e = 10^9/cc$) in this region, that is, the window, by water injection (ref. 11). Hence, the minimum depth of penetration in the radial direction was required to be to at least the depth at which $N_e$ decreased below the critical level (for a given signal frequency.) For the Gemini spacecraft a radial penetration of 0.9 the distance to the shock layer would be required (ref. 8). The minimum width of the window was taken to be $\lambda/2$ (where $\lambda$ is the wavelength of the transmitted signal), based on elementary waveguide theory, although it is shown in the appendix that propagation below normal waveguide cut-off is possible in lossy waveguides. However, as discussed in reference 12 and the appendix, signal recovery was expected to be directionally dependent since the diameter of the Gemini spacecraft and associated plasma sheath was large with respect to a VHF wavelength. Finally, the length of the window was assumed to be adequate as long as the region of reduced $N_e$ (below critical levels) extended over the antenna transmitting the signal.

With these estimates of the dimensions required for the window, mass flow requirements of water to reduce electron concentration below the critical level (for a given frequency) can be calculated. These calculations, which were performed in reference 7 using different assumptions, give results with considerable scatter for the required amounts of water. Hence, the injection program was designed to provide for a large range of flow rates (Maximum/Minimum = 25). The determination of the design levels of experiment parameters is given in subsequent sections.

### Gemini Spacecraft

The Gemini spacecraft reentry configuration is shown in figure 1. The overall length of the spacecraft is about 145 in. (368 cm) and the diameter at the heat-shield—spacecraft juncture is 90 in. (228.6 cm). Other spacecraft dimensions are indicated in the figure. The weight of the Gemini reentry configuration is of the order of 9000 lb (40 034 N).

The location of the three C-band antennas on the conical cabin section and the VHF systems antenna on the aft end of the spacecraft is shown in figure 1. The location of the compartment used for the water injection experiment system is also shown. This compartment is commonly referred to as the right main landing-gear well. A detailed description of the spacecraft is given in reference 9.

The spacecraft structure consisted of a titanium load-bearing frame containing an internal pressurized cabin and supporting systems which were covered by thermal insulation and a heat protection surface. Since the heat protection surface, particularly if it is ablative, can have an influence on the reentry plasma electron concentration, a brief description is given. (The effects of ablation products were not included in the experiment design and analysis (except for C-band) since the effects were expected to be small, especially in the inviscid layer.) The heat shield is made of a fiber-glass honeycomb core filled with a silicon elastomer ablator. The conical cabin portion of the spacecraft is covered with René 41 shingles 0.016 inch (0.041 cm) thick. The center cylindrical body and the conical afterbody, with the exception of the VHF antenna fairing, are covered with beryllium shingles of variable thickness. A detailed analysis of the effects of the Gemini heat shield ablation products on electron concentration is given in reference 9.

Attitude control of the spacecraft during flight is maintained by jets on the cylindrical portion of the spacecraft. These jets use the fuel monomethyl-hydrazine $(CH_2)N_2H_3$ and oxidizer nitrogen tetroxide $N_2O_4$; this information is included since the thrustors exhaust the chemical products of these fluids into the flow field.

## Gemini Reentry Environment and Experiment Geometry

The Gemini spacecraft center of gravity is off the axial center line; this forces the spacecraft to fly at an angle of attack and develop lift. Since the center of gravity is toward the bottom of the spacecraft (all directions are with respect to the astronauts), the bottom part of the spacecraft is tilted slightly toward the wind (and is called the windward side). The lift vector is directed towards the bottom of the spacecraft. By controlling the roll attitude of the spacecraft, the astronauts are therefore able to maneuver the spacecraft to some extent toward a desired landing point.

The Gemini spacecraft begins reentry with the heat shield facing forward and the astronaut's viewing window side (top) of the spacecraft normally facing down. This view of the spacecraft (from the south) is shown in the lower sketch of figure 2. For this orientation, the astronauts are heads down and flying backward. Since during this mission the spacecraft was being maneuvered, the Gemini spacecraft was banked 45° to the left at the start and throughout most of the blackout. This orientation of the spacecraft as viewed from the south side of the flight path is shown in the upper sketch of figure 2.

The bow shock typical of Gemini spacecraft flying at angle of attack is much more tightly wrapped around the windward side. (See fig. 2.) The flow field on the windward side of the spacecraft is "attached" so that an inviscid layer extends from the vehicle boundary layer out to the shock. However, the flow field on the leeward side of the spacecraft contains a separated-flow region. A complete description of the flow field is given in reference 9. It is most desirable to locate the injection nozzles on the windward side of the spacecraft, where water requirements should be least since the flow-field volume which is above $N_e$ critical is least.

The water injection system was actually installed on the right main landing-gear door about $28^{\circ}$ to the right of the windward side of the spacecraft. (See fig. 1.) This nonideal location was a result of guidelines requiring minimum interference with spacecraft structures and schedules. The water injection nozzles were placed toward the rear of the experiment compartment (fig. 1) and angled forward (at a $20^{\circ}$ angle with the spacecraft surface) to increase the dwell time of the water in the vicinity of the spacecraft and to allow the water jet more time to break up. Also, the distribution of water in the flow field as indicated by wind-tunnel test data (ref. 7) is shown in figure 2. The volume occupied by the water spray would be the communications window under idealized conditions.

It can also be seen from figure 2 that the roll attitude of the spacecraft was such that the injection nozzles were directed slightly away from the ground (about $15^{\circ}$ above the southern horizontal). This roll attitude was a result of other mission constraints and was not a preferred attitude to test water injection.

## Experiment Systems

Water injection system.- The onboard experiment consisted of a water injection system which was designed into the right main landing-gear door. Since the right main landing-gear door was completely removable, the system was completely independent of other spacecraft interfaces except for the electrical actuation switch and the leads to the astronauts' cabin. The gas pressurized water injection system is shown schematically in figure 3. The system was actuated by the right astronaut. A switch simultaneously released water expulsion pressure through the regulator to the water tank and started the mechanical timer. Once every 15 seconds the timer opened and closed contacts to each of three solenoid valves from which water was injected. This system was designed to produce pulses alternately of approximately 0.3-, 1.5-, and 7.5-lb/sec flow rate (0.14, 0.68, and 3.4 kg/sec) with durations of 1/2, 1/4, and 1/10 second. Figure 4 shows one typical ideal injection cycle. The water supply is depleted after about 12 cycles.

Figure 5 illustrates the exterior of the door covering the experiment compartment. The location of the door on the spacecraft and the nozzles on the door, a closeup of the

water injection nozzles, and data pertinent to the respective nozzles are shown. The injection orifices were essentially uniform bore holes drilled in insertable nozzles. The outer surface of these nozzles was normal to the injection orifices. The nozzles were directed forward so that the injection direction was about $20^{o}$ off the spacecraft surface. This arrangement was used to increase the dwell time of drops in the vicinity of the spacecraft. Figure 6 shows the experiment equipment installed on the inside of the right main landing-gear door. The electrical details of the system are presented in figure 7.

RF systems.- Three frequencies were in operation during reentry: VHF telemetry at 230.4 MHz, VHF voice at 296.8 MHz, and C-band at 5690 MHz. The VHF telemetry system transmitted a power of 2 W into a quarter-wave stub antenna with a gain of 2.5 dB over isotropic and a VSWR of about 2.1:1. The VHF voice system transmitted a power of 3 W into the same stub antenna with about the same gain and a VSWR of about 2.85:1. (During the injection period, the astronaut keyed the VHF voice transmitter to attempt communication on this link also.) The C-band radar transponder operates at 1-kW peak power which is fed to three helical antennas to form a circular roll pattern. The C-band signals were phase modulated to fill in nulls caused by interference between antennas.

Ground stations.- During the experiment operation period, ground stations near the reentry flight path (fig. 8) monitored signal strength on VHF telemetry, VHF voice, and C-band frequencies. Signal-strength monitoring capabilities at the various stations are listed in the following table:

| Station | Signal monitored | | |
|---|---|---|---|
| | VHF telemetry | VHF voice | C-band |
| Eglin Air Force Base | X | X | X |
| Mission Control Center at Cape Kennedy | X | X | |
| Telemetry Site II at Cape Kennedy | X | X | |
| Mila at Cape Kennedy | | | X |
| Patrick Air Force Base | | | X |
| Grand Bahama Island | X | | X |
| Grand Turk Island | X | | X |
| Anclote Point (Eglin AFB) | X | X | X |
| Key West (LRC van) | X | X | |
| Homestead (LRC van) | X | X | |
| Aircraft (4) | X | X | |

Design Estimates of Flight Parameters

Spray penetration and cross-sectional area.- In order to predict adequately the required amount of injectant flow rate, it is necessary to know the variation of injectant penetration and lateral dispersion during reentry. Studies were made in the Langley Mach 8 variable-density tunnel to predict the spray penetration and cross-sectional area during flight. These predictions have been previously reported in reference 7.

Under the conditions of fixed pressure and nozzle size, penetration could not be optimized throughout the blackout altitude range. For this reason, "design" altitudes were selected for each flow rate at which penetration was optimized. Penetration distance was chosen to extend almost to the bow shock at these altitudes by proper choice of nozzle size. Penetration for the high, medium, and low flow rates was designed to be optimum at 225 000 ft (68.58 km), 240 000 ft (73.15 km), and 262 000 ft (79.86 km), respectively. The altitude for optimum penetration for each nozzle was chosen to be the altitude at which the predicted flow rate required was equal to the actual flow rate injected.

The predicted variation in penetration with altitude for the conditions of the Gemini 3 flight is shown in figure 9. Shown also in this figure is the distance from the body to the shock (approximately where $N_e$ drops below the critical level), which is defined as the optimum penetration distance.

The design predictions for penetration were computed by assuming a nominal $15^o$ angle of attack $\alpha$ for the spacecraft during the reentry blackout. During the actual Gemini 3 flight, the angle of attack was $9^o$ instead of the nominal $15^o$. As a result, the penetration distance required at a given altitude was recomputed for the lower angle of attack and is also shown in figure 9. A comparison of these results indicates that the penetration distance required at a given altitude is greater for $9^o$ angle of attack.

It is seen that penetration decreases rapidly with a decrease in altitude. At higher-than-design altitudes, penetration would be large, and inefficient use of the water would result. At lower-than-design altitudes, penetration would be insufficient to open a window through the entire plasma sheath.

The lateral dispersion was also observed in a series of wind-tunnel tests (ref. 7). Scaling of these results to the flight model indicated that injection would cause a lateral distribution of water in the vicinity of the VHF antenna, which would cover an angle of about $60^o$ to $90^o$ and would be centered about the plane of the injection nozzle. Therefore, it was concluded that the lateral distribution of water was adequate to open a slot greater than the minimum required width of 1/2 VHF wavelength.

Flow rate required.- The design estimates of flow rate required to reduce $N_e$ below $10^9$/cc in the inviscid air plasma were previously reported in reference 7 and are

briefly reviewed herein. These estimates were determined by calculating the amount of water required to cool the inviscid air below a critical temperature (associated with critical $N_e$), with the assumption of equilibrium chemistry. It is shown in reference 3 that, although evidence indicates that $N_e$ depletion corresponding to signal recovery is caused by recombination of electrons and ions at the surface of water droplets (heterogeneous mechanisms) rather than a cooling mechanism (ref. 13 for theory), the assumption of equilibrium may be used to make engineering estimates of flow rate required.

The initial estimates of water flow rate required were based on the assumption of complete evaporation of the water injected. On the basis of these calculations, flow rates of 0.3, 1.5, and 7.5 lb/sec (0.14, 0.68, and 3.4 kg/sec) were selected as the flight test flow rates. It was subsequently determined that the water injected does not completely evaporate. Hence, the effect of incomplete evaporation on the design flow rate estimates was considered (ref. 7).

Calculated results of the effects at the VHF antenna site of incomplete evaporation of water injected at the design flow rates (at the "optimum" penetration design altitude) are summarized from reference 7 in the following table:

| Flow rate | | Design altitude | | Percent evaporated | $N_e$/cc |
|---|---|---|---|---|---|
| lb/sec | kg/sec | ft | km | | |
| 7.5 | 3.40 | 225 000 | 68.58 | 30 | $4 \times 10^7$ |
| 1.5 | .68 | 240 000 | 73.15 | 30 to 40 | $10^9$ |
| .3 | .14 | 262 000 | 79.86 | 25 to 35 | $10^{10}$ |

On the basis of these calculations, it was therefore expected that at the respective design altitudes, water injection at the high flow rate would cause signal recovery; however, the medium flow rate would be marginal and the low flow rate would be too small to give signal recovery.

VHF radiation characteristics of communications window.- An experimental investigation was undertaken to determine the radiation characteristics of the VHF stub antenna in the presence of a slotted plasma sheath. The objective of this investigation was to obtain measurements of pattern beam width and radiation field intensity in order to (1) evaluate the effectiveness of the material addition window in restoring communications and (2) optimize the location of the tracking stations in relation to the spacecraft entry attitudes. The results of this study (analysis given in the appendix) are shown in the radiation contour plots of figures 10(a) and 10(b). The predicted signal levels in decibels are given relative to the peak free-space value (0 dB, the reference gain of a half-wavelength dipole). Figure 10(a) gives the roll-plane pattern characteristics from $\phi = 0^o$ to $\phi = 180^o$ (aperture at $\phi = 90^o$) and defines the radiation field for stations

to the south of the flight path. In figure 10(b) the pattern is continued from $\phi = 180^{o}$ to $\phi = 360^{o}$ and shows the radiation field for stations to the north of the flight path. By plotting station look angles on the contours, a signal profile was obtained for each tracking station. It is evident from these plots that the south stations should receive substantial signal recovery due to the orientation of the window in that direction. The stations to the north, however, with the exception of Grand Bahama Island, are looking to the back side of the window and therefore should show only marginal signal recovery.

## RESULTS

### Reentry Events and Conditions

The variations with time from lift-off of reentry altitude and velocity and of reentry angle of attack and roll attitude are shown in figures 11 and 12, respectively. The reentry flight path was previously shown in figure 8. In these figures, special reference is made to times important to the experiment. VHF blackout began at 4:39:59 (hour:minute:second elapsed from lift-off) at an altitude of about 318 000 ft (96.93 km). At about 4:36:26 (3 min 33 sec before blackout), the spacecraft executed a left roll of approximately $45^{o}$, which placed the injection nozzles about $75^{o}$ south of straight up or about $15^{o}$ above the horizontal. The spacecraft remained at this attitude until about 4:43:40 when the roll angle was reduced to approximately zero (fig. 12); this caused the injection nozzles to point about $30^{o}$ south of straight up. The experiment was actuated at 4:41:16 (1 min 17 sec after blackout began) at an altitude of 272 000 ft (82.90 km), and it ended 3 min later at an altitude of 160 000 ft (48.77 km). VHF blackout ended at 4:45:00 at an altitude of 134 000 ft (40.84 km). Angle of attack which was predicted to be a nominal $15^{o}$ during this period was much lower than expected. The maximum angle of attack, as seen in figure 12, was about $10^{o}$.

### Water Flow Rates

The flow rate of the water injection system was determined by preflight calibration and was not monitored in real time. Twelve cycles of three different flow rates from 0.3 to 7.5 lb/sec (0.14 to 3.4 kg/sec) were employed over the data period. The flow rate sequence was shown previously in figure 4. The mission times (time from lift-off) at which flow rate pulses started are given in table I. Pulse times during the first 45 sec and the last minute of the injection period were verified by signal-strength pulses; the remaining pulse times were determined by extrapolation.

TABLE I.- STARTING TIMES OF FLOW RATE PULSES

| Cycle | Time, hr:min:sec, of – | | |
|---|---|---|---|
| | Low flow rate pulse | Medium flow rate pulse | High flow rate pulse |
| 1 | 4:41:15.9 | 4:41:19.9 | 4:41:24.6 |
| 2 | 4:41:31.2 | 4:41:35.2 | 4:41:39.9 |
| 3 | 4:41:46.5 | 4:41:50.5 | 4:41:55.2 |
| 4 | 4:42:01.8 | 4:42:05.8 | 4:42:10.5 |
| 5 | 4:42:17.1 | 4:42:21.1 | 4:42:25.8 |
| 6 | 4:42:32.4 | 4:42:36.4 | 4:42:41.1 |
| 7 | 4:42:47.7 | 4:42:51.7 | 4:42:56.4 |
| 8 | 4:43:03.0 | 4:43:07.0 | 4:43:11.7 |
| 9 | 4:43:18.3 | 4:43:22.3 | 4:43:27.0 |
| 10 | 4:43:33.6 | 4:43:37.6 | 4:43:42.3 |
| 11 | 4:43:48.9 | 4:43:52.9 | 4:43:57.6 |
| 12 | 4:44:04.2 | 4:44:08.2 | 4:44:12.9 |

Duration of pulses: Low, 0.46 sec; medium, 0.21 sec; high, 0.10 sec

## Signal-Strength Measurements

The signal-strength records from Langley vans at Key West and Homestead, Fla., aircraft 3, aircraft 4, and Grand Bahama Island show that significant levels of signal recovery were observed on VHF telemetry and VHF voice corresponding to the high flow rate pulses during the early portion of the water injection sequence. The latitude and longitude and altitude when pulses were noted are shown in figures 8 and 11. In figure 13, plots of VHF signal strength against time show two well-defined signal-recovery pulses plus a less definitive third one received at the Key West station. Each signal-strength pulse corresponds to a high flow rate water pulse. Signal-recovery results from all stations are given in table II. Aircraft 3, aircraft 4, and Grand Bahama Island stations did not receive the third signal-recovery pulse. No VHF signal recovery was received during the low and medium flow rate injections. No VHF signal recovery was observed at any stations other than those listed in table II.

Signal-strength records from Mila (Cape Kennedy, Fla.) and Grand Bahama Island C-band radars show signal-strength enhancement pulses corresponding to the latter portion of the injection sequence. The level of signal-strength increase indicates that the signal was not greatly attenuated. The C-band signal-strength oscillograph record obtained at Grand Bahama Island is shown in figure 14. The record is broken so that each line is one injection period long. The time during which injection occurs is indicated.

TABLE II.- VHF SIGNAL RECOVERY (DECIBELS)

| Station | Receiver[1] | Receiver noise level | High flow rate pulse | | |
|---|---|---|---|---|---|
| | | | Cycle 1 | Cycle 2 | Cycle 3 |
| Key West | Telemetry | 0.25 μV | 25 dB | 26 dB | 25 dB |
| | Voice | .25 μV | 20 dB | 23 dB | 25 dB |
| Homestead | Telemetry | .04 μV | 22 dB | 27 dB | Trace |
| | Voice | .13 μV | 10 dB | 22 dB | Trace |
| Grand Bahama Island | Telemetry | .20 μV | 15 dB | 17 dB | |
| Aircraft 3 | Telemetry | .18 μV | 10 dB | 5 dB | |
| Aircraft 4 | Telemetry | .13 μV | | 5 dB | |

[1]Telemetry frequency, 230.4 MHz; voice frequency, 296.8 MHz.

Pulses of significant level can be seen corresponding to the medium and high flow rate water pulses. The stations at Grand Bahama Island and Mila were tracking in the beacon mode. The other Cape Kennedy radar was tracking in the skin-track mode and consequently did not record any enhancement pulses. The C-band radar records at Eglin Air Force Base did not show these enhancement pulses. Anclote Point C-band data are inconclusive since the time correlation of the signal-strength record with the experiment injection pulses could not be established.

## DISCUSSION OF VHF SIGNAL-STRENGTH RESULTS

Signal-strength results show that the Gemini VHF signal which had been completely blacked out was increased to a high level above receiver noise by water injection. The significance of these results is that the water injection technique of radio signal attenuation alleviation has been shown to work for a body of the size, shape, and velocity of Gemini, which is typical of current manned reentry spacecraft.

Although the design range of water injection parameters was not adequate to maintain VHF signal recovery over the entire blackout period, the high degree of signal recovery obtained down to 245 000 ft (74.68 km) demonstrates the applicability of material addition techniques to blunt-type spacecraft. The inability to maintain communications at the lower altitudes with the design range of injection parameters was analyzed from a fluid mechanics (ref. 8) and electromagnetic standpoint and it appears that the following factors are involved:

(1) Insufficient injection penetration – The increase in the shock layer thickness due to the lower than predicted angle of attack would have required injection penetration greater than provided. Insufficient penetration would result in an electromagnetic window of inadequate depth. The altitudes when injection pulses occurred are plotted on the

penetration prediction plot (fig. 9); it can be seen that penetration (based on the actual $9^{o}$ angle of attack) was marginal at the altitude where the fourth recovery pulse would have occurred and was thereafter insufficient.

(2) Unknowns of the Gemini flow field – The addition of ablative products containing metals of low ionization potential are known to cause the electron concentration in the flow field to increase. The electron concentration due to ablation products in the separated-flow and shear layers on the leeward side of Gemini was calculated to be higher than the corresponding inviscid $N_e$ in references 9 and 10. Also, the location of the VHF antenna in a separated-flow wake region could conceivably contribute to lower-than-predicted recovery levels. (See refs. 7, 8, and 10.)

(3) Unfavorable aspect angle – Since signal recovery was very dependent on vehicle aspect angle (see section beginning on p. 13), it is conceivable that minor deviations in vehicle aspect caused by flight could contribute to loss of VHF signal recovery. For example, for the Key West and Homestead stations, roll aspect angle increased from about $20^{o}$ off ideal receiving attitude during the second large flow rate pulse to about $30^{o}$ off ideal receiving attitude during the third such pulse.

(4) Insufficient persistance of the VHF communications window – Since the Gemini VHF antenna is about 8 ft (243.8 cm) downstream of the injection site, diffusion of electrons into the spray region and decreasing density of the spray with distance could result in a window of insufficient length. In the appendix it is shown that if the window does not extend to the VHF antenna (slot length = $3\lambda$), signal recovery is greatly reduced. A similar decrease in effectiveness of water addition with distance aft was noted on the RAM B2 flight test (ref. 3), where three antennas were located from 2 to 10 ft (60.9 to 304.8 cm) downstream of the injection site.

Although the reasons for the decrease of VHF signal recovery are not conclusively known, the period during which signal recovery was recorded provides an opportunity to construct and examine theoretical predictions, using measured flight results for comparison.

## Comparison of Calculated and Observed Electron Concentration During Water Injection

Computations of the electron concentration in the inviscid flow during the high flow rate injection pulses were compared with the electron concentrations deduced from VHF signal attenuation in reference 8. It is indicated in references 9 and 10 that the electron concentration in the shear layer and in the aft separated-flow region in the vicinity of the VHF antenna may be greater than that in the inviscid layer. However, since injection

took place only on the windward side where the flow is largely attached, the shear layer would be smaller and its effect on VHF communications is presumably less important. Also, temperature measurements during water injection tests reported in reference 7 indicate that ample cooling due to water injection occurs in the aft separated region to reduce the electron concentration below critical for VHF.

The resulting plot of peak electron concentrations at the VHF antenna station during the high flow rate water injection as a function of altitude is reproduced from reference 8 in figure 15. Solid lines are faired through solutions to theoretical computations which included the effect of both droplet surface and the usual recombination mechanisms, whereas dashed lines are faired through a solution in which only the effect of droplet surface recombination was considered. The altitudes where the first four high flow rate water injection pulses occurred are denoted in the figure. A horizontal line at $N_e = 10^9/cc$ represents the approximate critical value of $N_e$ for VHF communications. It is seen that for both calculations, electron concentration is well below critical $N_e$ for the first two high flow rate pulses and somewhat greater than critical $N_e$ for the third and fourth pulses. These results compare favorably with the observations that signal recovery was strong for the first two high flow rate injections, marginal for the third, and undetectable from then on. Although many assumptions about the spray and flow-field conditions are required to make a calculation of this type, the results seem to indicate the proper trend.

## Comparison of VHF Flight Signal Strength Measurements With Ground Simulation Measurements

In order to determine the degree of VHF signal recovery, it was necessary to use free-space patterns of the scale model to calculate the reference level for each tracking station. This was necessary because the tracking stations were unable to acquire a reference signal from the Gemini spacecraft prior to blackout. The comparisons of the measured signal-recovery levels with those predicted on the basis of the simulation are given relative to the computed free-space signal reference level in figure 16.

The three recovery pulses observed occurred over an altitude range from 262 000 to 245 000 ft (79.86 to 74.68 km) and were obtained for the high flow rate. Key West and Homestead, however, were the only stations to record recovery during the third pulse (table I). The predictions for Key West show close agreement with actual signal-recovery levels. At Homestead, the first recovery pulse is 6 to 8 dB below predicted level; whereas, in the second pulse, the 296.8-MHz recovery is within 1 dB and the 230.4-MHz recovery is within 4 dB of the predicted recovery. Aircraft 3 received only the 230.4-MHz signal and shows a recovery of -20 dB and of -27 dB for the first pulse and second pulse,

respectively, which are somewhat below the predicted level. Aircraft 4 also received only the 230.4-MHz signal and recorded only the second recovery pulse which is 5 dB above predicted level. At Cape Kennedy and Anclote Point, no recovery was observed. The predicted recovery levels of -30 dB (first pulse) and -27 dB (second pulse) for Cape Kennedy and -35 dB and -26 dB for Anclote Point, however, indicate that signal recovery would be marginal. Grand Bahama Island only tracked the 230.4-MHz signal which is approximately 3 dB higher recovery than predicted. Since Grand Turk Island and aircraft 6 were not within tracking range during this portion of the experiment, results for these stations are not included. Although a high recovery level was predicted for Eglin AFB, no recovery pulses were observed. During the three pulses, however, the station look angle was such that the propagation path included a large section of the wake which was not accounted for in the simulation tests.

It therefore appears that the antenna pattern simulation predicted the general behavior of the radiation characteristics while recovery was observed, that is, the time the communications window was open. On this basis, Gemini VHF signal recovery at a ground station is strongly dependent on the location of the communications window in the vicinity of the line of sight to this ground station. Further, as pointed out in the appendix, signal recovery is greatly reduced if the length of the communications window is much less than $3\lambda$ (about 9 ft (274 cm)).

## C-BAND ATTENUATION AND RECOVERY

The signal-strength records show that C-band signal attenuation was observed at altitudes between 200 000 and 160 000 ft (60.96 and 48.77 km) and that signal-strength enhancement occurred for both medium and high flow rate pulses. Since C-band signal was not blacked out, these results indicate that the electron concentration during periods of no injection was about $4 \times 10^{11}$/cc, which is critical $N_e$ for C-band. At these altitudes, alleviation of VHF attenuation, which would have required reduction of $N_e$ below $10^9$/cc, did not occur.

Calculations of the finite rate chemistry (ref. 10) show that the electron concentration in the Gemini inviscid flow is insufficient to explain any attenuation of C-band signal. However, reference 10 indicates that the electron density interior to the inviscid flow in the separated-flow and shear layers can greatly exceed the levels in the inviscid flow.

An analysis of the C-band results of this experiment was presented in reference 10, which showed that the observed attenuation may well have been caused by ionized ablation products in the separated zone of the flow field. In figure 17 this concept is used to explain the signal recovery noted. In this figure, the calculated $N_e$ levels in the inviscid flow (lower curve) and the electron concentration observed during this and previous

Mercury flights (upper curve) are plotted against altitude. The analysis of reference 10 concludes that the electron concentration observed in flight without water addition during C-band attenuation is due to the separated-flow region (corresponds to the upper curve in fig. 17). The altitudes at which water was injected and signal was recovered are indicated. As previously stated, VHF recovery was achieved for the first three high flow rate pulses at stations on the south only, between altitudes of 272 000 and 246 000 ft (82.90 and 74.98 km). Since $N_e$ is above critical for VHF in both the inviscid and separated-flow plasmas, the water injected must penetrate through both plasmas to produce recovery. When penetration became insufficient to reduce $N_e$ in the outer layers of the inviscid plasma, the VHF signals were blacked out. Later, the separated-flow $N_e$ became large enough for C-band attenuation. As has been shown, recovery is noted on C-band for these times at stations north of the flight path, which were the only C-band beacon tracking stations available during this portion of the reentry.

The attenuation and recovery of C-band signal indicate that, although penetration is not sufficient to relieve the inviscid plasma $N_e$ below critical for VHF, the electron concentration in the separated region is being reduced below the critical C-band level. The recovery of C-band signal from the north supports this belief. Diffusion and mixing in the separated region would allow the spreading of material addition completely throughout this region, and since this region shields all three C-band antennas from the north stations, the recovery from the north is thus explained (ref. 10). Inasmuch as the inviscid plasma mixing is confined to a rather narrow sector of flow, any signal recovery due to injection, when this plasma is above critical, would be directional so that little or no signal recovery would have been observed by the north stations.

## CONCLUDING REMARKS

A flight test has been conducted to determine if radio attenuation during hypersonic flight can be alleviated by injection of water into a narrow sector of the flow field. The test vehicle was the Gemini 3 spacecraft. Attenuation levels with and without water injection were recorded during the reentry portion of this flight on frequencies of 230.4, 296.8, and 5690 MHz over a range of altitudes from 350 000 to 160 000 ft (106.68 to 48.77 km) and a range of velocities from 24 200 to 15 000 ft/sec (7.376 to 4.572 km/sec).

From the signal-strength data obtained, the following remarks can be made:

1. Signal recovery was achieved during parts of the experiment data period on both VHF and C-band and, therefore, it is possible to alleviate radio attenuation on a blunt body by water injection into a narrow slot in the flow field.

2. The variation with altitude of electron concentration during water injection calculated by a method which assumes the primary mechanism for signal recovery is

recombination of electrons and ions at the surface of water drops shows the same trend as that of the electron concentration deduced from the VHF signal recovery.

3. VHF signal-recovery radiation pattern is in good agreement with the radiation pattern obtained under simulated flight conditions. From simulation and flight results it was predicted and verified that the signal would be beamed in the radial direction of water injection.

4. The C-band signal attenuation was probably caused by ionized ablation products in the separated and shear layers of the flow field.

5. The loss of the VHF communications window at altitudes below 245 000 ft (74.68 km) was probably due to inadequate injection penetration caused by off-nominal vehicle attitude.

Langley Research Center,
National Aeronautics and Space Administration,
Langley Station, Hampton, Va., August 18, 1967,
125-21-02-09-23.

# APPENDIX

## EXPERIMENTAL DETERMINATION OF EFFECTS OF A SLOTTED PLASMA SHEATH ON RADIATION CHARACTERISTICS OF THE GEMINI STUB ANTENNA

By Francis P. Russo and Aubrey E. Cross
Langley Research Center

This appendix presents numerical results of the analytical studies and ground simulation tests to determine the radiation properties of the Gemini VHF stub antenna shrouded by a slotted plasma sheath.

### Symbols

| | |
|---|---|
| $d$ | shroud diameter |
| $E_z(r,\phi)$ | electric field (polar coordinates) z-component |
| $H_r(r,\phi)$ | radial magnetic field (polar coordinates) |
| $H_\phi(r,\phi)$ | circumferential magnetic field (polar coordinates) |
| $l_A$ | aperture length |
| $N_e$ | electron concentration |
| $TE_1, TE_2$ | first and second transverse electric modes |
| $t$ | sheath thickness |
| $w_A$ | aperture width |
| $w_S$ | slot width |
| $\delta$ | loss tangent |
| $\epsilon'$ | relative dielectric constant |
| $\theta$ | spherical coordinate angle between a vector and Z-axis |
| $\lambda$ | free-space wavelength |
| $\sigma$ | complex conductivity |

## APPENDIX

$\phi$ spherical angular coordinate in XY (roll) plane

$\omega$ signal frequency in free space, radians

$\omega_p$ plasma frequency, radians

### Antenna Test Model and Radiation Coordinate System

A 1/18-scale modeling system was selected on the basis of providing reasonable model sizes and availability of test equipment in the corresponding frequency range. The 4800-MHz test frequency was obtained by scaling the mean value for the 230.4-MHz and 296.8-MHz spacecraft frequencies. The scaled model of the Gemini spacecraft is shown in figure 18. The model was constructed of 3/32-inch-thick (0.238 cm) copper and contained a 4800-MHz 14-mW continuous-wave oscillator and power supply. The 4800-MHz antenna was a one-quarter wavelength stub with a gain of 2.5 dB above isotropic.

The radiation coordinate system of the antenna model is shown in figure 19. The spherical angular coordinates $\phi$ (in the XY-plane) and $\theta$ (in the Z, constant $\phi$ plane) define the roll and yaw planes, respectively. The roll patterns were obtained by rotating the model about the Z-axis with the initial slot position at $\phi = 0^o$ and the receiver located on the X-axis. The yaw patterns shown in the appendix were obtained by placing the slot initially at $\phi = 90^o$ and then rotating the model about the X-axis, with the receiver located on the Z-axis. Other pattern measurements were made in the yaw plane for $5^o$ increments in roll to obtain radiation contours for the model. Signal-strength measurements were made with a RHC (right-hand circular) helix receiving antenna having a $39^o$ beam width and 8-dB gain.

### Plasma Sheath Simulation

Under the Gemini entry environment in which the electron density in the ionized flow surrounding the stub antenna is above $N_e$ critical at VHF, there will be negligible RF energy leakage through the plasma sheath. Consequently, for the slotted plasma sheath, the power density in the far radiation field will be determined primarily by the transmission properties of the slot. Under these conditions a reasonable simulation of the slotted plasma sheath could be obtained by the use of high loss dielectrics geometrically scaled to the reentry environment. The materials used to simulate the absorptive properties of the plasma sheath consisted of polyester resins impregnated with 50 percent graphite by weight. This mixture produced an absorber with a relative dielectric constant $\epsilon'$ of 9 and loss tangent $\delta$ of 0.9 at the 4800-MHz test frequency.

To obtain pattern measurements in relation to sheath thickness and aperture size, the shroud configurations in figure 20 were utilized. The shroud diameter d is chosen

so that the wall thickness corresponds to the thickness of the sheath $t$ surrounding the antenna, which is assumed opaque to RF energy. Although the shroud configuration for $d/\lambda = 2$ is a close simulation of the actual region of high signal losses, the cases of $d/\lambda = 4$ and $d/\lambda = 5$ were included in order to determine the pattern sensitivity to sheath thickness. The geometry of the window in relation to the spacecraft, which is shown in figure 21, was obtained from the water droplet spray profile studies of reference 7. To determine the effects of variations in window size, measurements were made for aperture lengths of $2\lambda$, $3\lambda$, and $4\lambda$ and for aperture widths of $\lambda$, $1.5\lambda$, and $2\lambda$. Since preliminary measurements had shown that the patterns were relatively insensitive to variations in aperture width, further tests were limited to the $1.5\lambda$ aperture which corresponds to the width of the predicted window.

## Theoretical Analysis of Slotted Plasma Sheath

A theoretical analysis of radiation from slotted plasma sheaths has been made at the University of Michigan (ref. 12) for the purpose of determining the radiation field produced by spacecraft antennas in relation to plasma window size, sheath thickness, and plasma conductivity. The mathematical model assumed applicable for plasma sheaths on the order of a wavelength or greater in thickness is shown in figure 22. Basically, the model consists of an electric line source of unit electric current along the Z-axis that is shrouded by a concentric plasma sheath of thickness $t$ with an axial slot of width $w_S$. The electromagnetic properties of the sheath are described by a complex conductivity $\sigma$ that is assumed uniform throughout the medium. It is also assumed that the plasma frequency $\omega_p$ is sufficiently high so that there is negligible RF leakage through the unslotted sheath. By opening a window in the sheath, the electric line source is able to set up electric fields in the slot which couple energy from the source to free space. This transfer of power can be analyzed in terms of lossy waveguide concepts for specific propagation modes. In figure 23 is shown the cut-off and propagating boundaries of the two lowest order modes in relation to plasma frequency and normalized slot width. For narrow slots the analysis can be confined to the solution of the first propagation mode $(TE_1)$ in which the nonzero components for the electric field are $E_Z(r,\phi)$ and for the magnetic field are $H_r(r,\phi)$ and $H_\phi(r,\phi)$. It is evident from figure 23 that the $TE_1$ mode will propagate through slots less than a half-wavelength in width when the sheath losses are small. By determining the transverse electric field in the plasma slot the radiation field can be computed by the use of Green's function which entails the assumption that the electric field in the cylindrical surface is negligible. The radiation field for the theoretical model is given in figure 24 for sheath thicknesses $t$ of $\lambda/2$ and $2\lambda$ and a slot width $w_S$ of $\lambda/2$. The plasma frequency $\omega_p$ and electron—neutral-particle collision frequency were assumed to be equal to twice the transmission frequency. It is evident that the radiation field becomes more directional as the sheath

thickness exceeds the free-space wavelength. The patterns in figure 25 are for a sheath thickness of $3\lambda$ with slot widths of $\lambda$ and $\lambda/2$. It is seen that the slot in the cylindrical plasma sheath produces only a main forward lobe with half-power beam widths on the order of $75^{\circ}$ for the half-wavelength slot and $50^{\circ}$ for the 1-wavelength slot.

## Results of Pattern Simulation Tests

The free-space pattern characteristics of the scale model are given in figure 26. The roll pattern indicates that the radiation field is fairly symmetrical about the vehicle although, as seen from the yaw pattern, there is a dropoff of approximately 15 dB in the vicinity of the nose and tail. The roll and yaw patterns of the simulated plasma sheaths are given as a function of sheath thickness in figure 27 and figure 28, respectively, for an aperture length $l_A$ of $3\lambda$. The peak and average signal levels are given relative to the free-space patterns (dash-line curves). Comparison with the free-space patterns shows that the large sheath surrounding the spacecraft antenna results in substantial signal beaming in the direction of the window at $\phi = 0^{\circ}$ with very little radiation on the back side of the window. These results are in agreement with the theoretical patterns of figure 25. These results also indicate that increasing the sheath thickness above $2\lambda$ produces little change in the beam-width characteristics, which are similar to those produced by a large ground plane. Polar plots of signal strength as a function of sheath thickness are presented in figure 29 for an aperture length $l_A$ of $4\lambda$.

Typical patterns showing the effects of aperture length on the recovery characteristics are given in figures 30 and 31 for a sheath thickness of $2\lambda$. Although some recovery is observed for $l_A = 2\lambda$, it is evident that a minimum aperture length of $3\lambda$ is required for significant recovery levels. Although these results show that the window is effective in reestablishing radiation, the directive characteristics of the antenna patterns indicate that the window orientation relative to the ground tracking stations would have a major influence on the received signal level. This effect is clearly illustrated in figure 32 in which relative signal level is plotted as a function of vehicle roll angle for a broadside look angle ($\phi = 90^{\circ}$). It is seen that the signal strength on the back side of the window is 25 dB below the peak value. The approximate beam widths are $50^{\circ}$ at -3 dB, $80^{\circ}$ at -6 dB, and $180^{\circ}$ at -15 dB. A three-dimensional plot of the radiation field was obtained from the anticipated window length of $4\lambda$ and for a sheath thickness of $2\lambda$. The radiation field with the window at $\phi = 90^{\circ}$ is shown in figure 10 as a contour plot in which signal level in dB is given relative to the peak free-space value.

REFERENCES

1. Sims, Theo E.; and Jones, Robert F.: Flight Measurements of VHF Signal Attenuation and Antenna Impedance for the RAM A1 Slender Probe at Velocities up to 17,800 Feet Per Second. NASA TM X-760, 1963.

2. Russo, F. P.; and Hughes, J. K.: Measurements of the Effects of Static Magnetic Fields on VHF Transmission in Ionized Flow Fields. NASA TM X-907, 1964.

3. Cuddihy, William F.; Beckwith, Ivan E.; and Schroeder, Lyle C. (With appendix A by Ivan E. Beckwith, Dennis M. Bushnell, and James L. Hunt; appendix B by Ivan E. Beckwith and Sadie P. Livingston; appendix C by Ivan E. Beckwith): Flight Test and Analysis of a Method for Reducing Radio Attenuation During Hypersonic Flight. NASA TM X-1331, 1967.

4. Gemini Mission Evaluation Team: Gemini Program Mission Report GT-3. Gemini 3. MSC-G-R-65-2, NASA, Apr. 1965.

5. Schroeder, Lyle C.: Gemini Reentry Communications Experiment. NASA Paper presented at Third Symposium on the Plasma Sheath (Boston, Mass.), Sept. 21-23, 1965.

6. Schroeder, Lyle C.; Sims, Theo E.; and Cuddihy, William F.: Experiment T-1, Reentry Communication on Gemini III. Manned Space Flight Experiments Symposium – Gemini Missions III and IV, NASA, Oct. 1965, pp. 81-103.

7. Beckwith, Ivan E.; Bushnell, Dennis M.; and Huffman, Jarrett K.: Investigation of Water Injection on Models of Gemini Vehicle and Resulting Predictions for GT-3 Reentry Communications Experiment. NASA TM X-1200, 1966.

8. Beckwith, Ivan E.; Bushnell, Dennis M.; and Huffman, Jarrett K.: Fluid Mechanics Aspects of the Gemini Reentry Communications Experiment. Conference on Langley Research Related to Apollo Mission, NASA SP-101, 1965, pp. 217-237.

9. Anderson, P. J.; Fivel, H. J.; Fox, J. F.; Grose, G. G.; Hickerson, J. L.; Joerger, C. D.; Kessler, W. C.; Mattox, D. L.; and Young, D. E.: The Effect of Ablation Products on Gemini Reentry Communications. Final Report. Rept. E467 (Contract No. NASw-1209), McDonnell Aircraft Corp., Apr. 1966.

10. Huber, Paul W.: Deduction of Reentry Plasma Properties About Manned Orbital Spacecraft From Radio Signal Attenuation Data. NASA TN D-4118, 1967.

11. Huber, Paul W.; and Sims, Theo E.: The Entry-Communications Problem. Astronaut. Aeron., vol. 2, no. 10, Oct. 1964, pp. 30-40.

12. Olte, Andrejs: The Radiation Pattern of an Electric Line Current Enclosed by an Axially Slotted Plasma Sheath – II. [Rept.] 5825-6-T (NASA Grant NsG-472), College Eng., Univ. of Michigan, Feb. 1966.

13. Evans, John S.: Charge Recombination on Water Droplets in a Plasma. NASA TM X-1186, 1965.

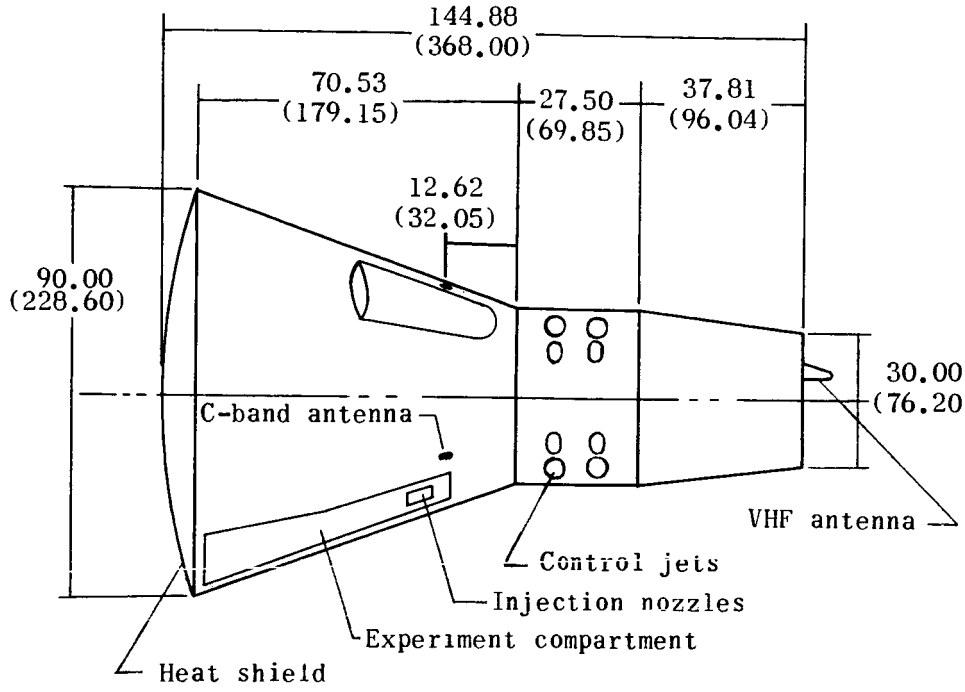


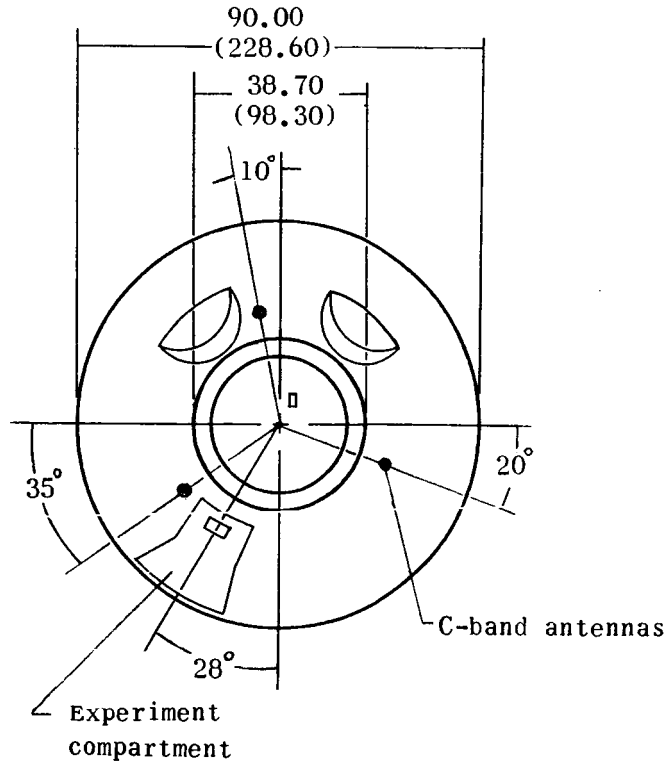


Figure 1.- Gemini spacecraft reentry configuration. (All dimensions are in inches (centimeters) unless otherwise indicated.)

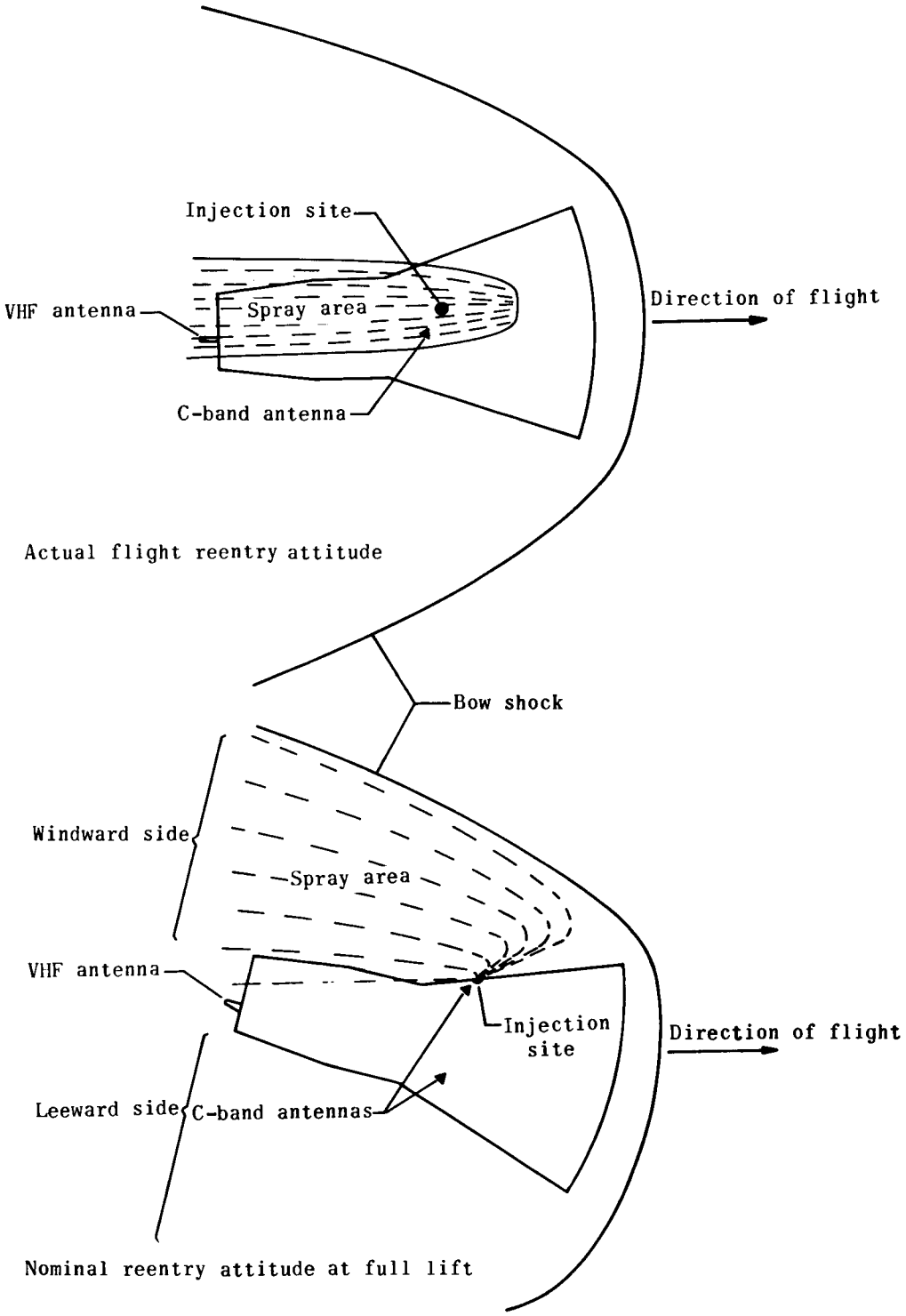


Figure 2.- Experiment geometry.

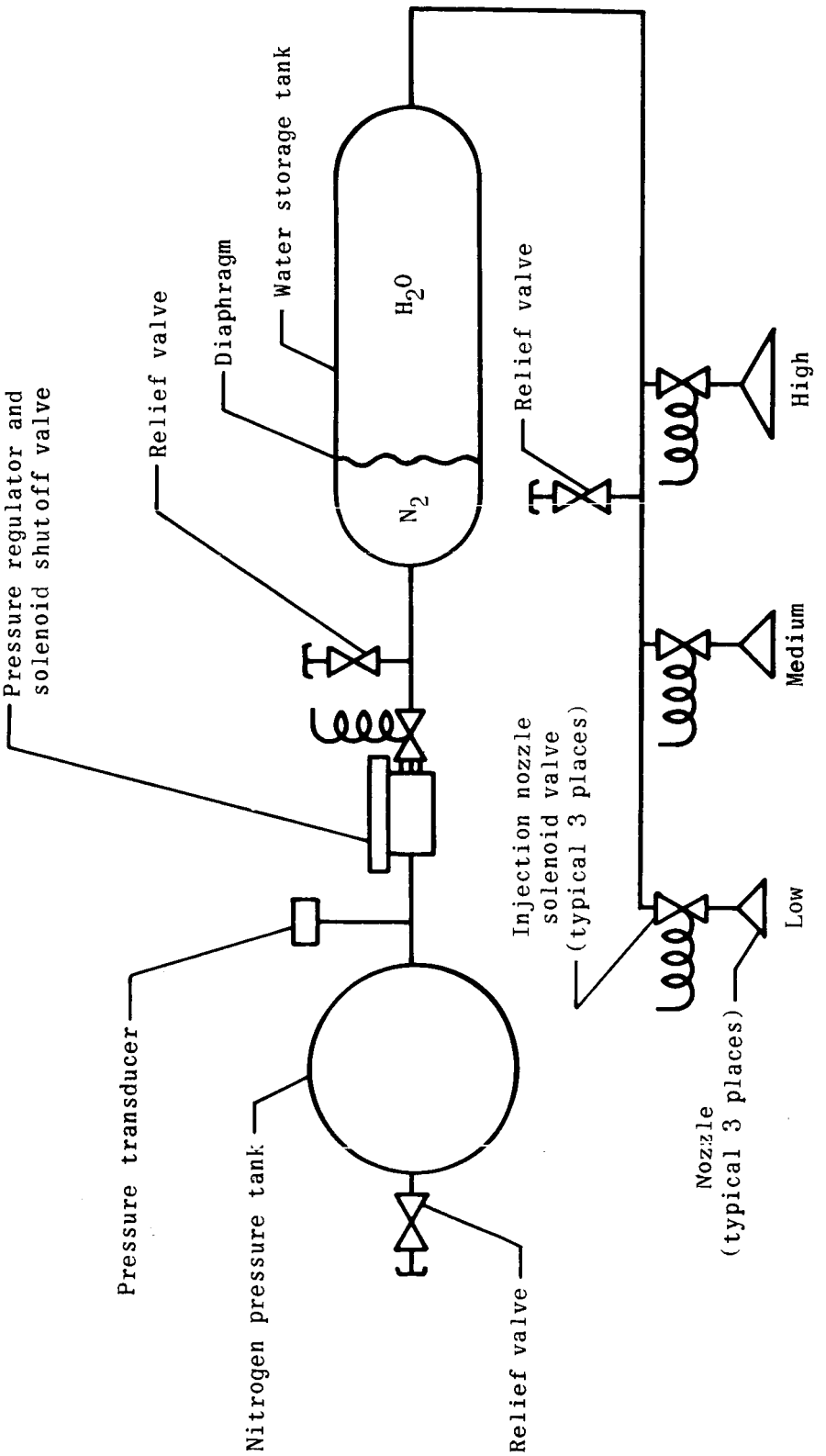


Figure 3.- Schematic of Gemini reentry communications experiment.

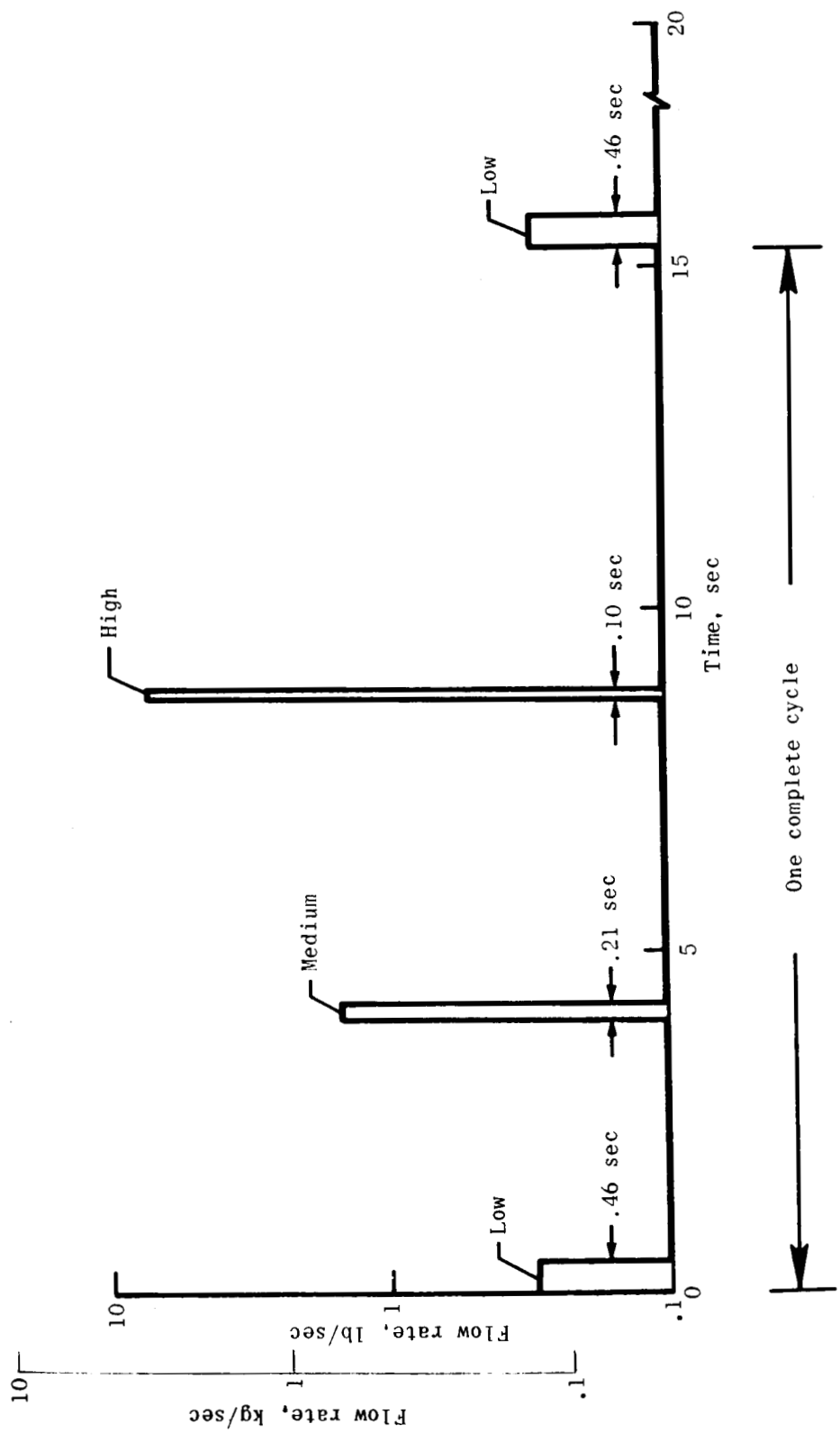


Figure 4.- Design flow rate cycle for Gemini reentry communications experiment.

Orifice Details

| Flow rate | | Number of orifices | Diam. of orifices | | Orifice length-diam. ratio | Injection velocity | |
|---|---|---|---|---|---|---|---|
| lb/sec | kg/sec | | in. | cm | | ft/sec | km/sec |
| 0.3 | 0.14 | 1 | .082 | .208 | 3.0 | 110 | 33.5 |
| 1.5 | 0.68 | 1 | .228 | .579 | 3.0 | 84 | 25.6 |
| 7.5 | 3.40 | 4 | .221 | .561 | 3.4 | 128 | 39.0 |

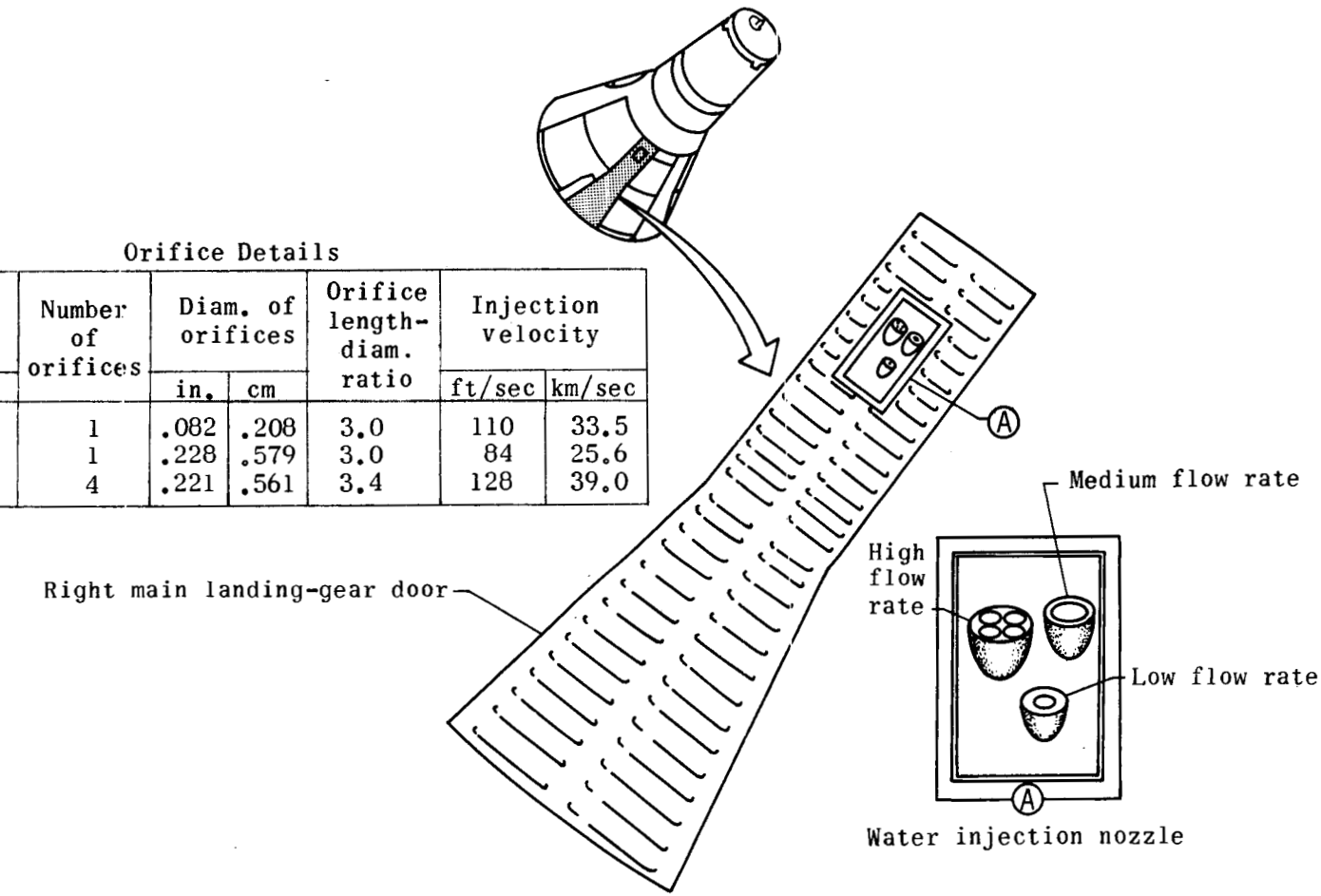


Figure 5.- Details and locations of injection nozzles for reentry communications experiment on Gemini spacecraft.

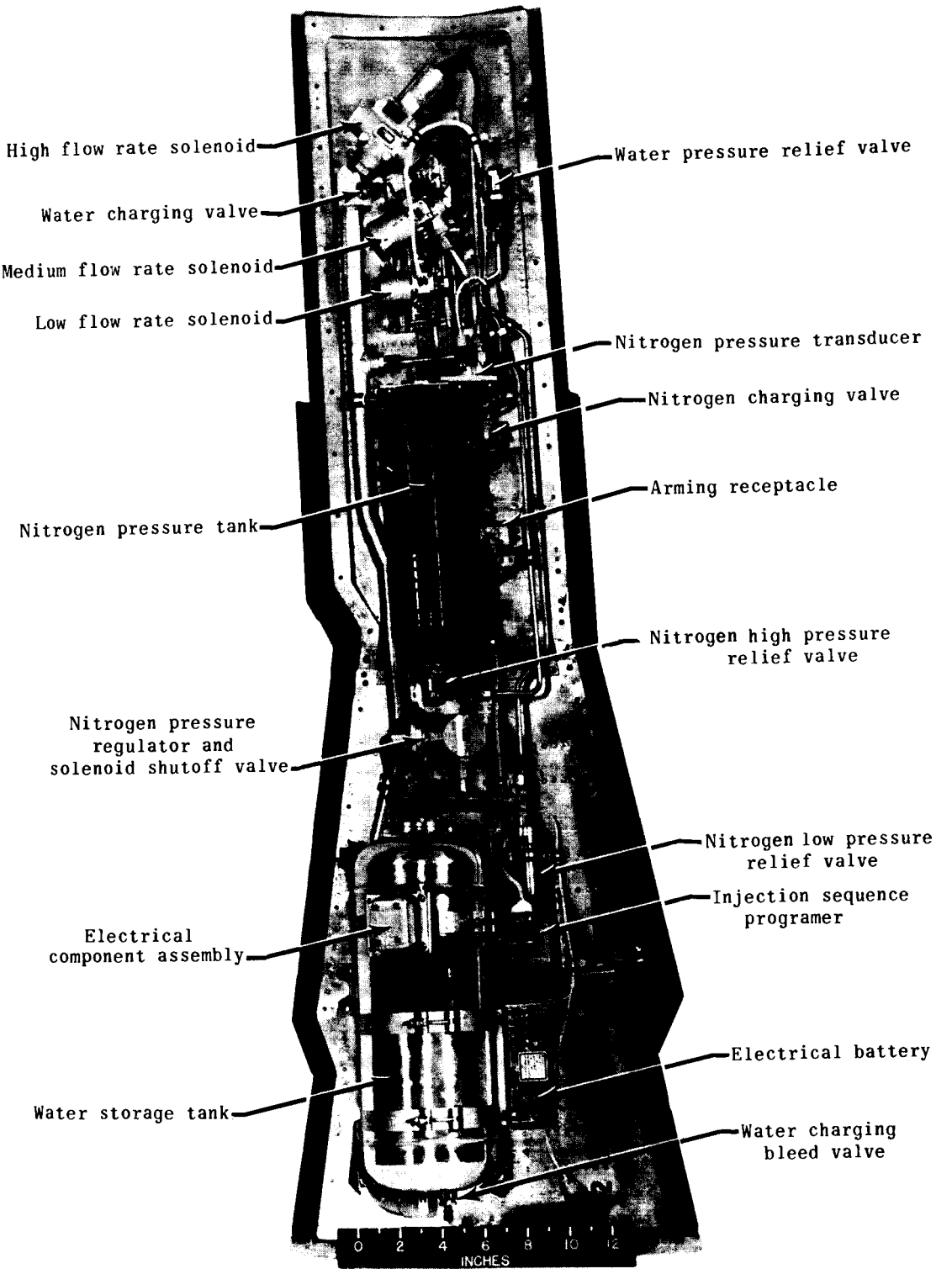


Figure 6.- Reentry communications experiment equipment on inside of right main landing-gear door.

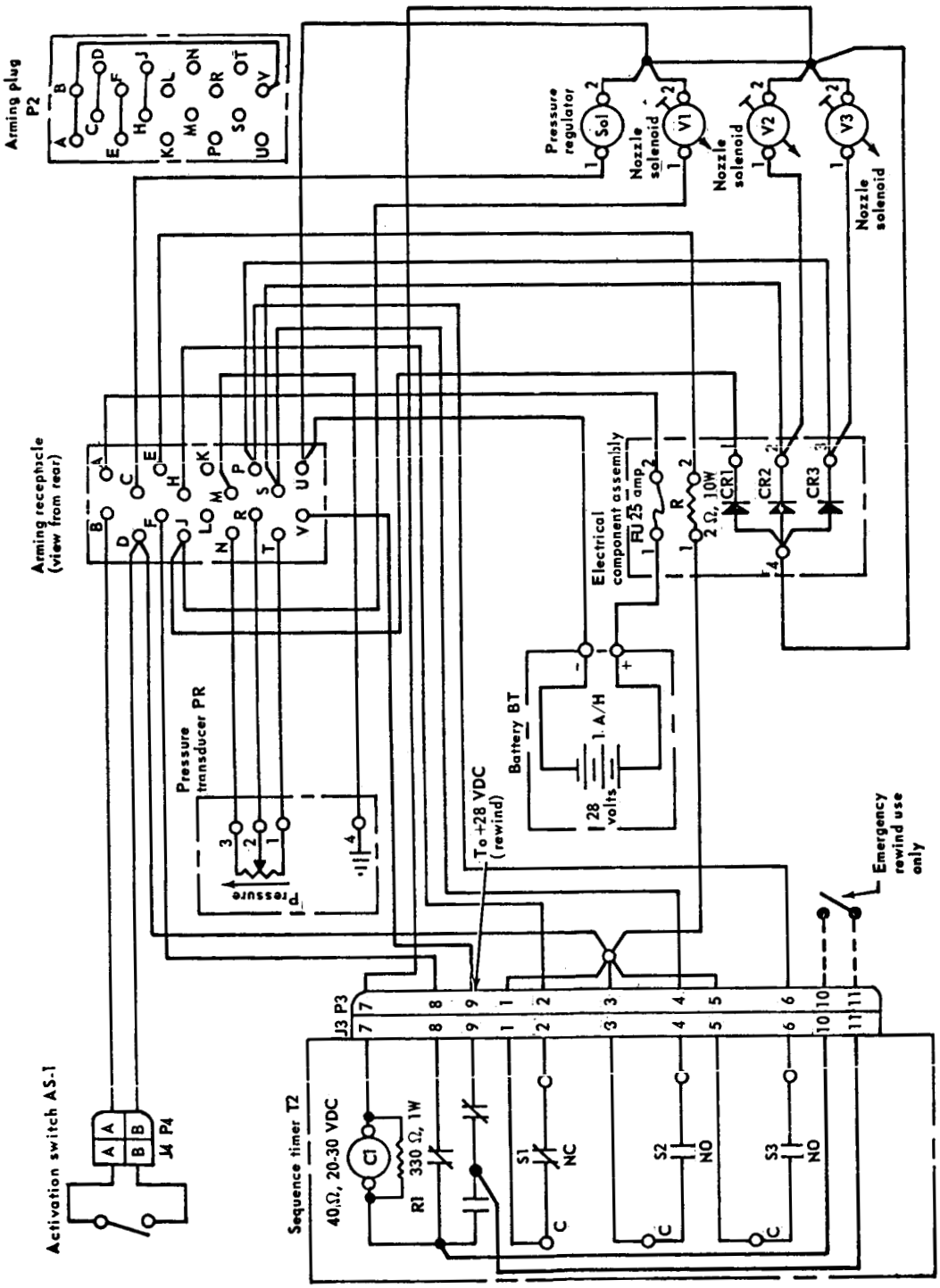


Figure 7.- Reentry communications experiment wiring diagram.

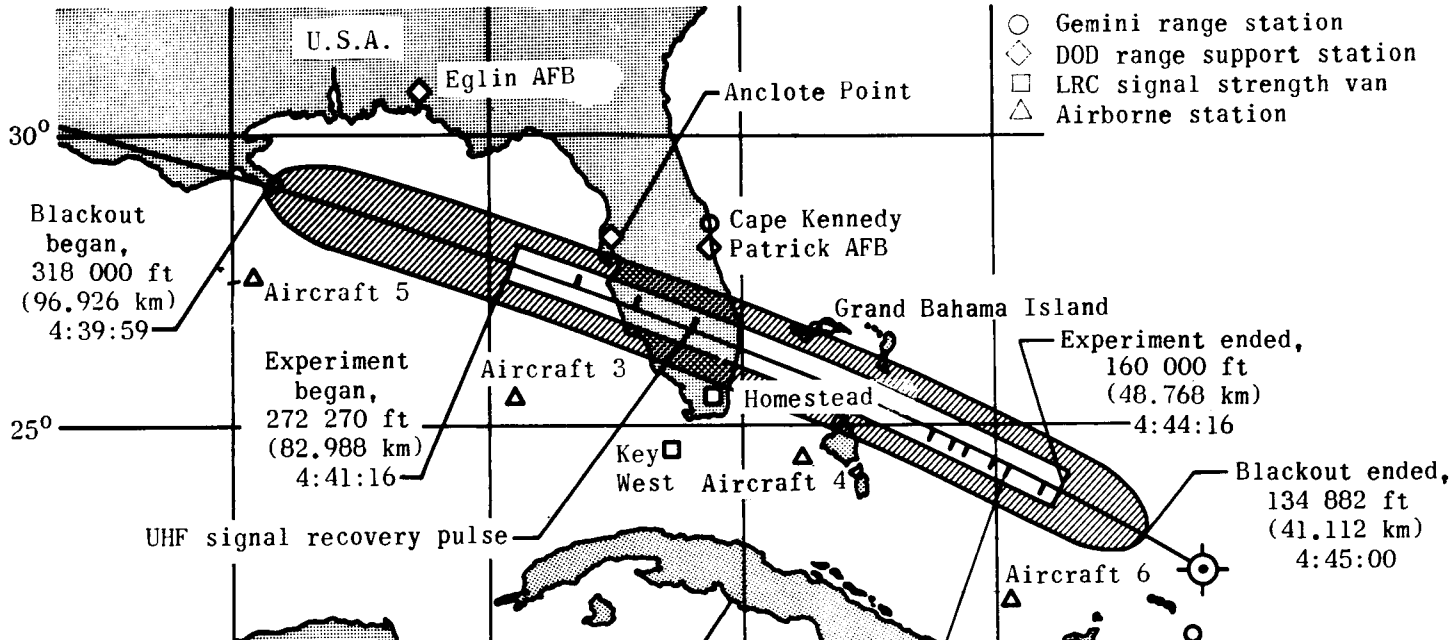


Figure 8.- Ground stations for Gemini reentry communications experiment.

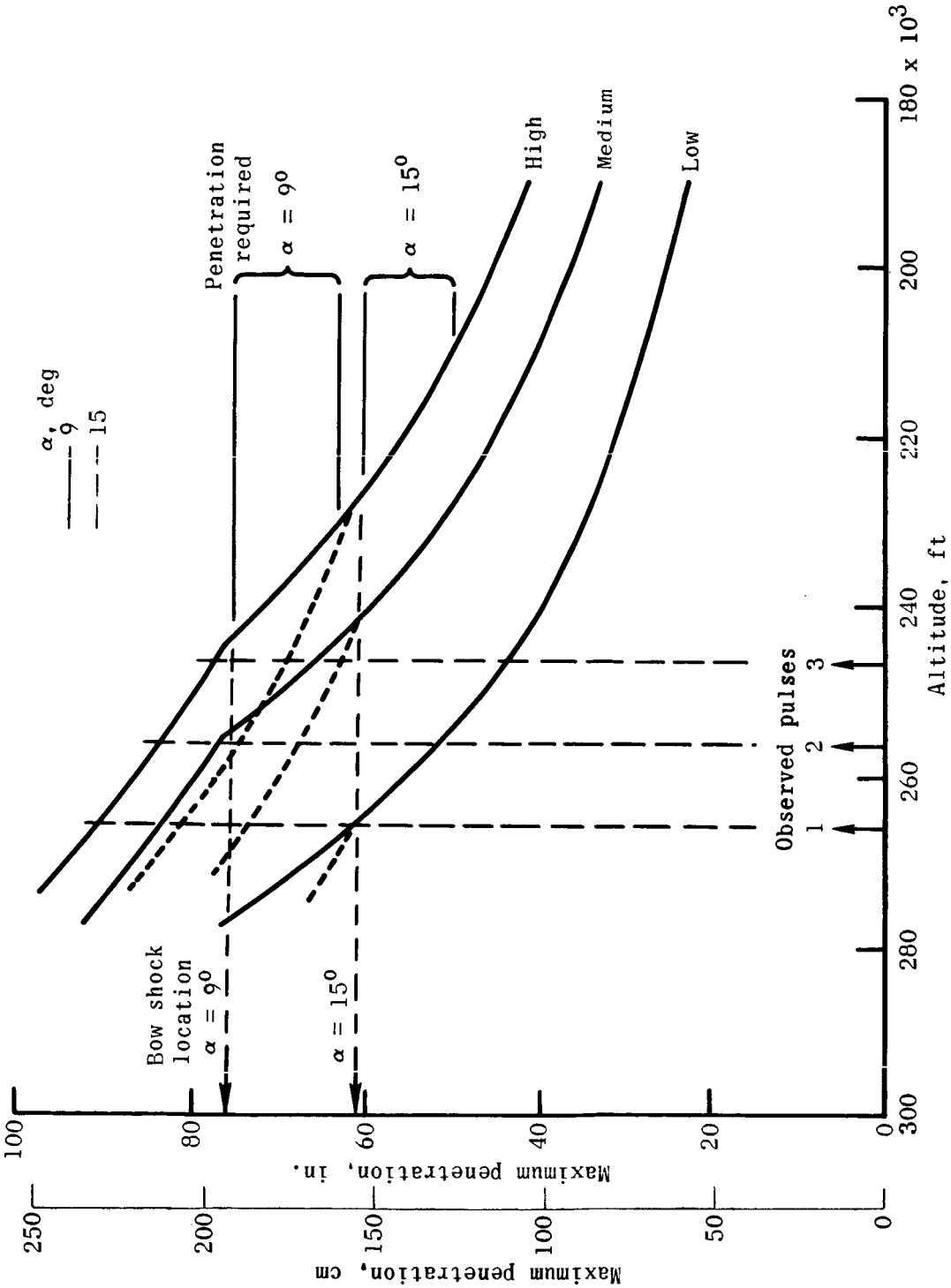


Figure 9.- Predicted maximum injectant penetration at VHF antenna site.

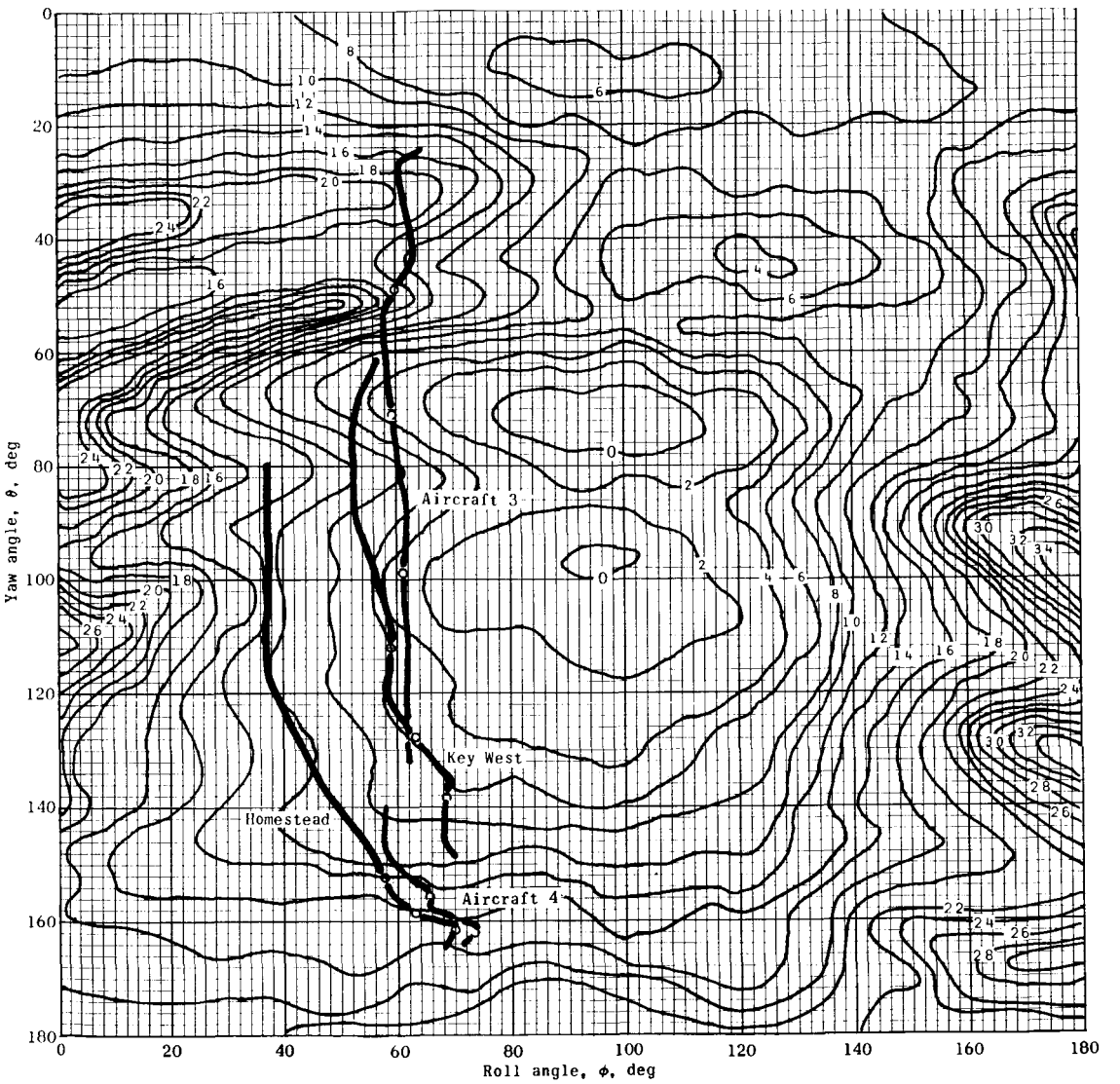


(a) Receiving stations south of flight path.

Figure 10.- Radiation field for the anticipated electromagnetic window.

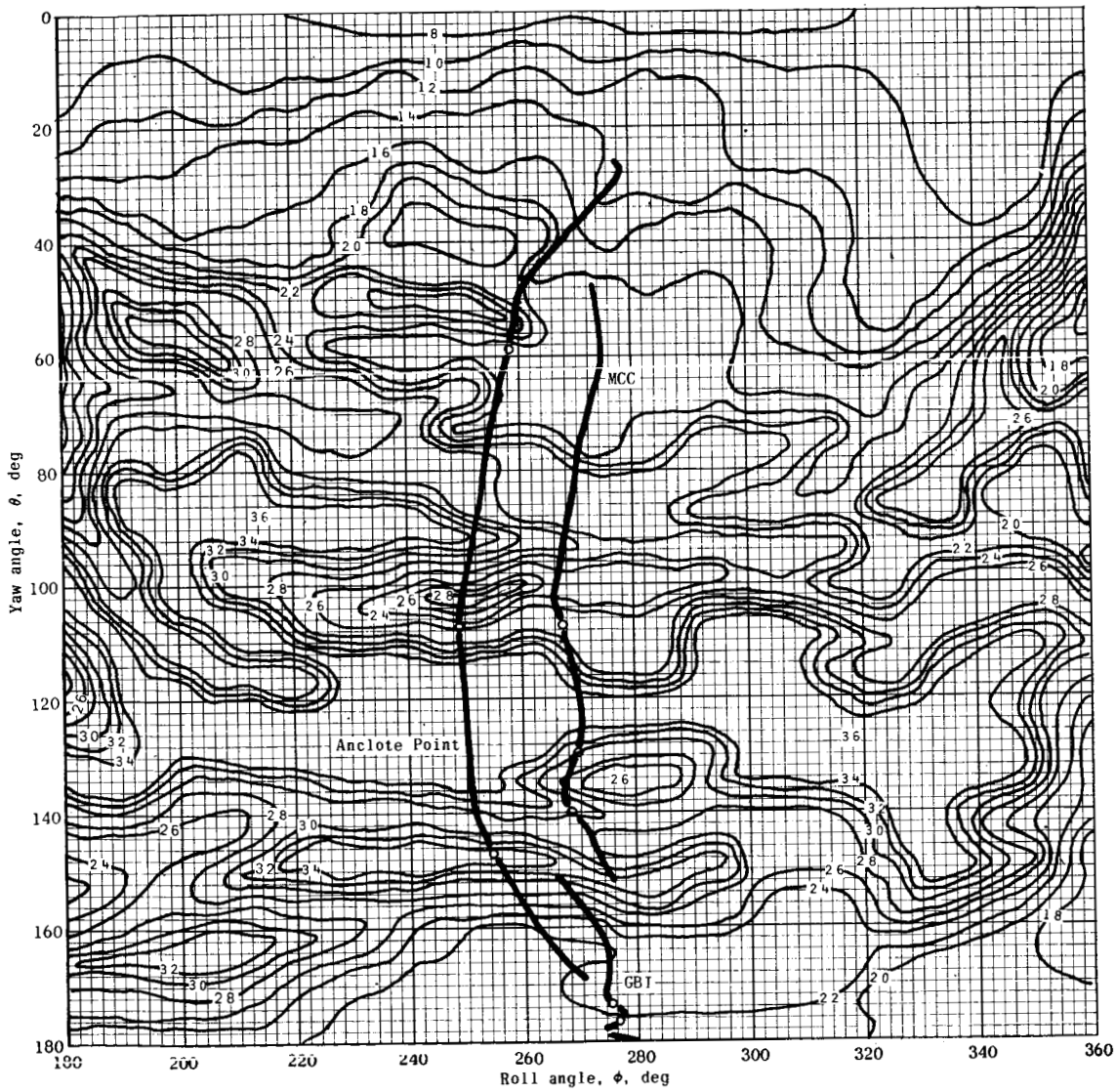


(b) Receiving stations north of flight path.

Figure 10.- Concluded.

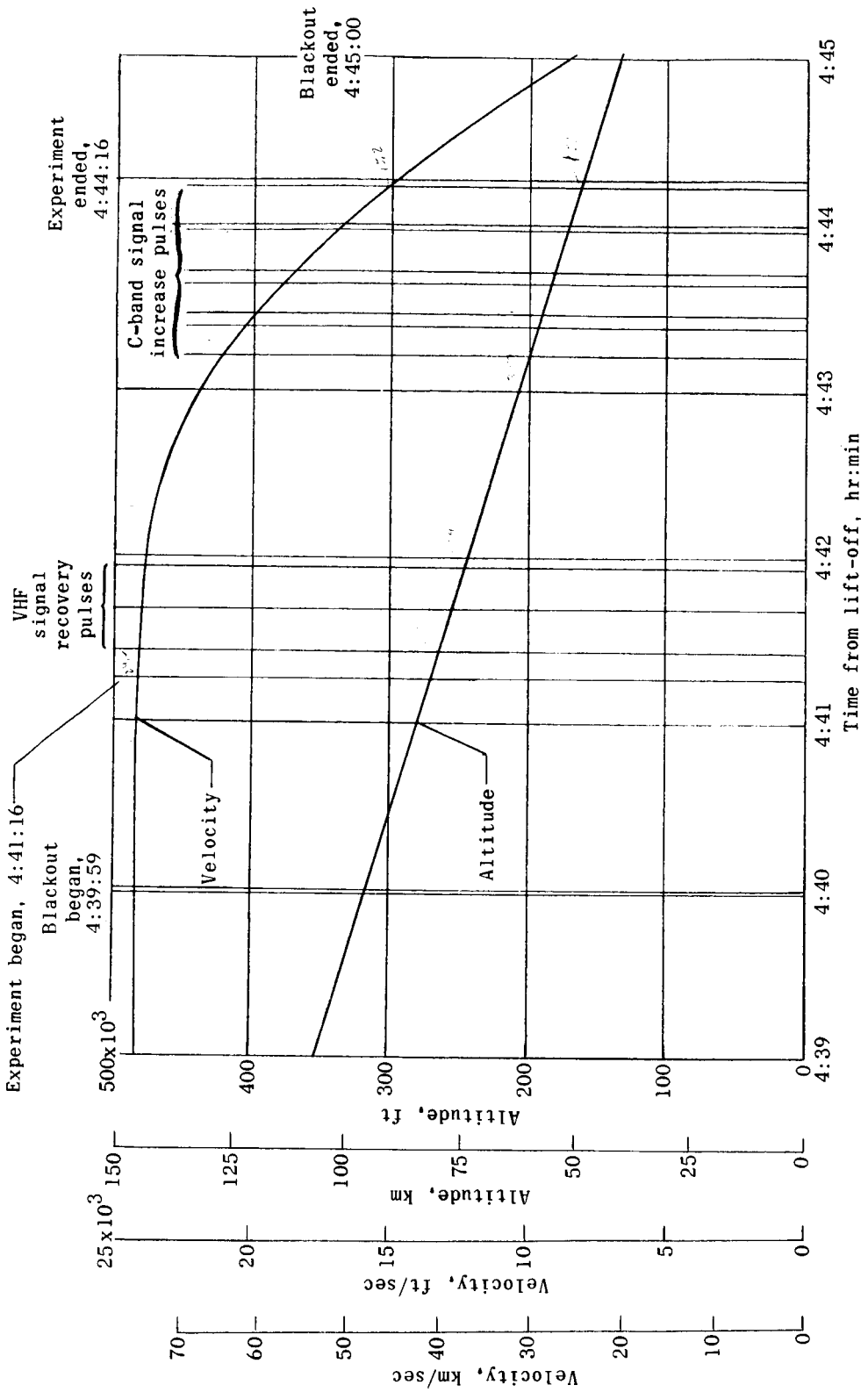


Figure 11.- Altitude and velocity as a function of time from lift-off.

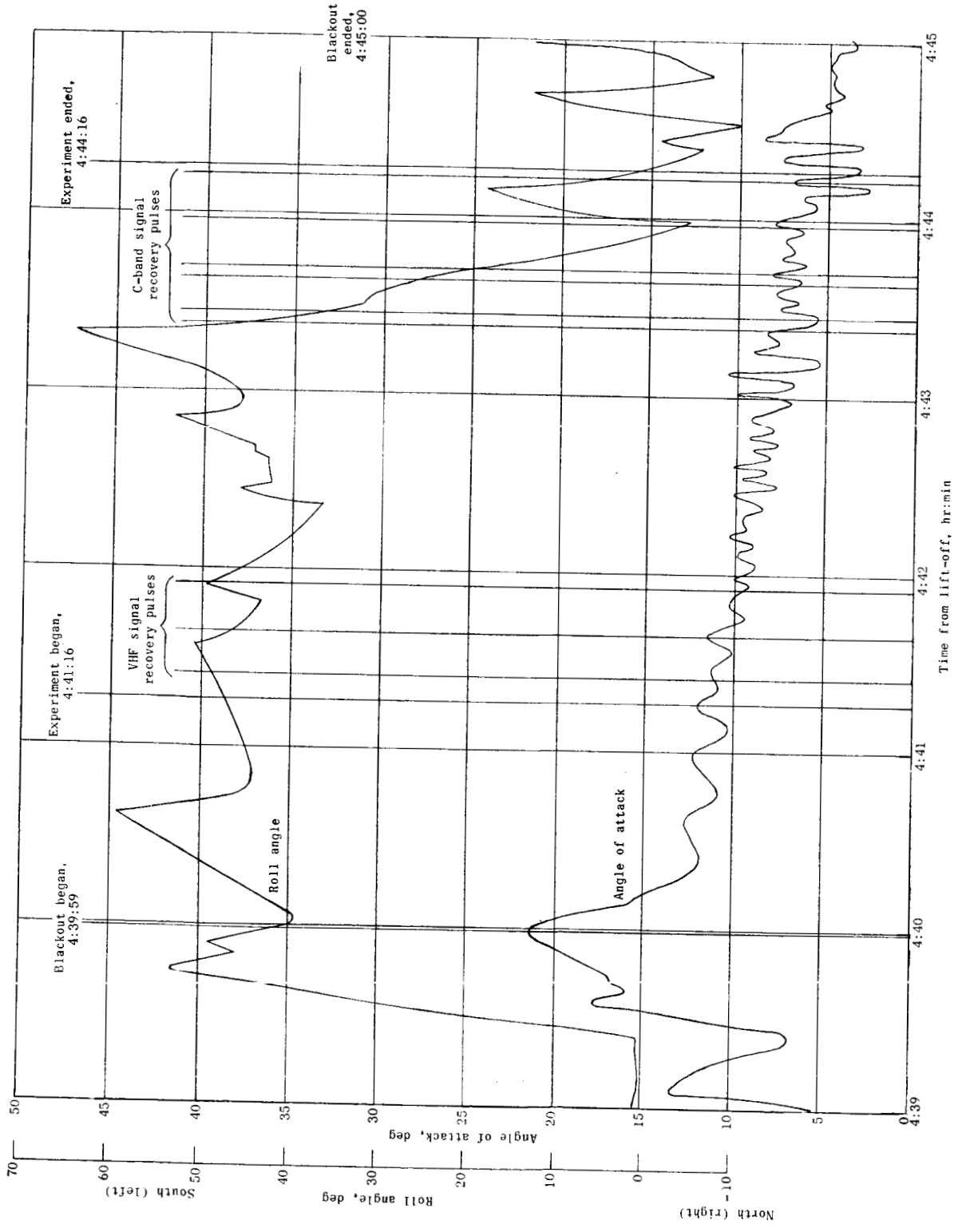


Figure 12.- Reentry angle of attack and roll angle as a function of time from lift-off.

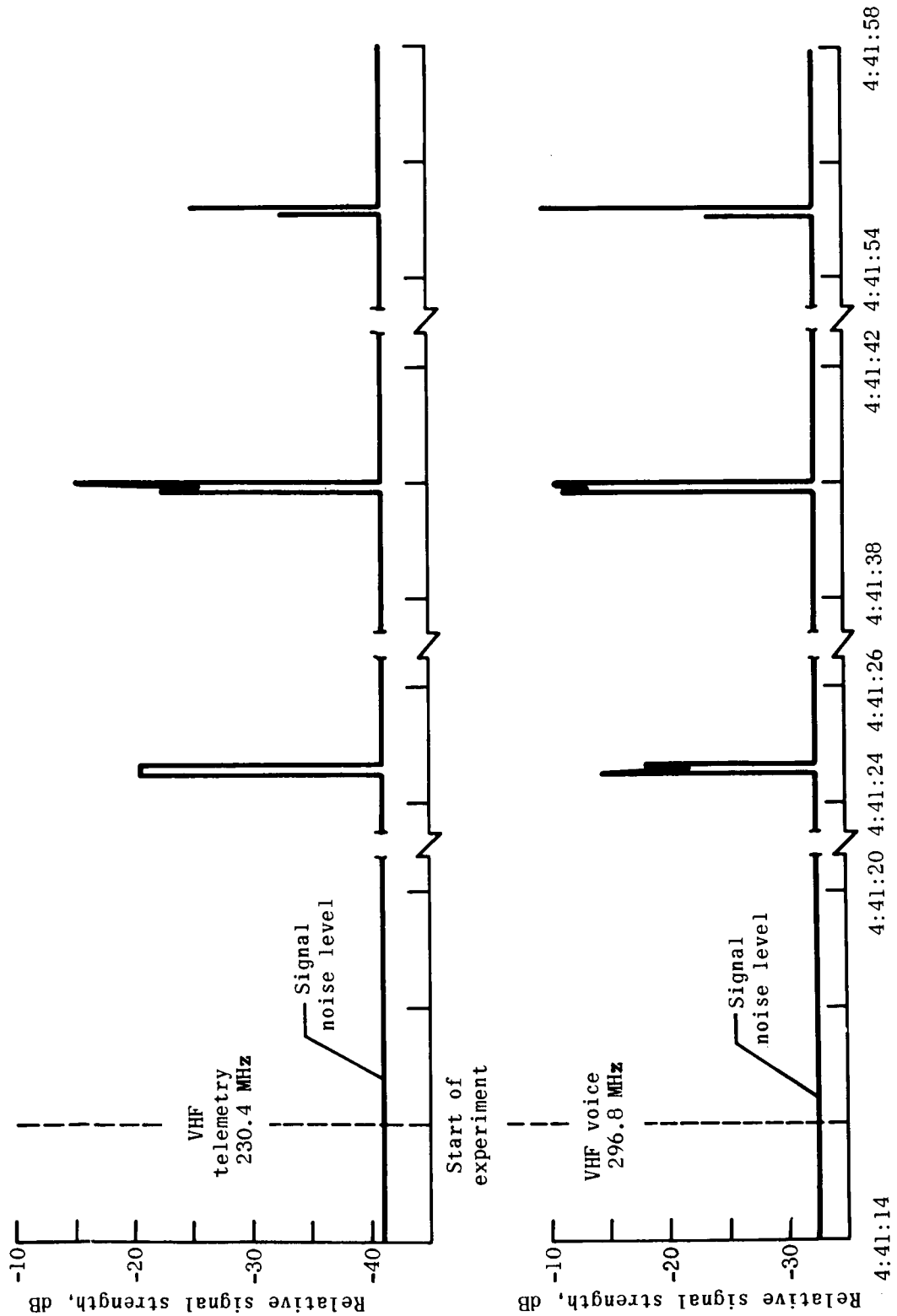


Figure 13.- Variation of VHF signal strength with time at LRC station at Key West, Florida.

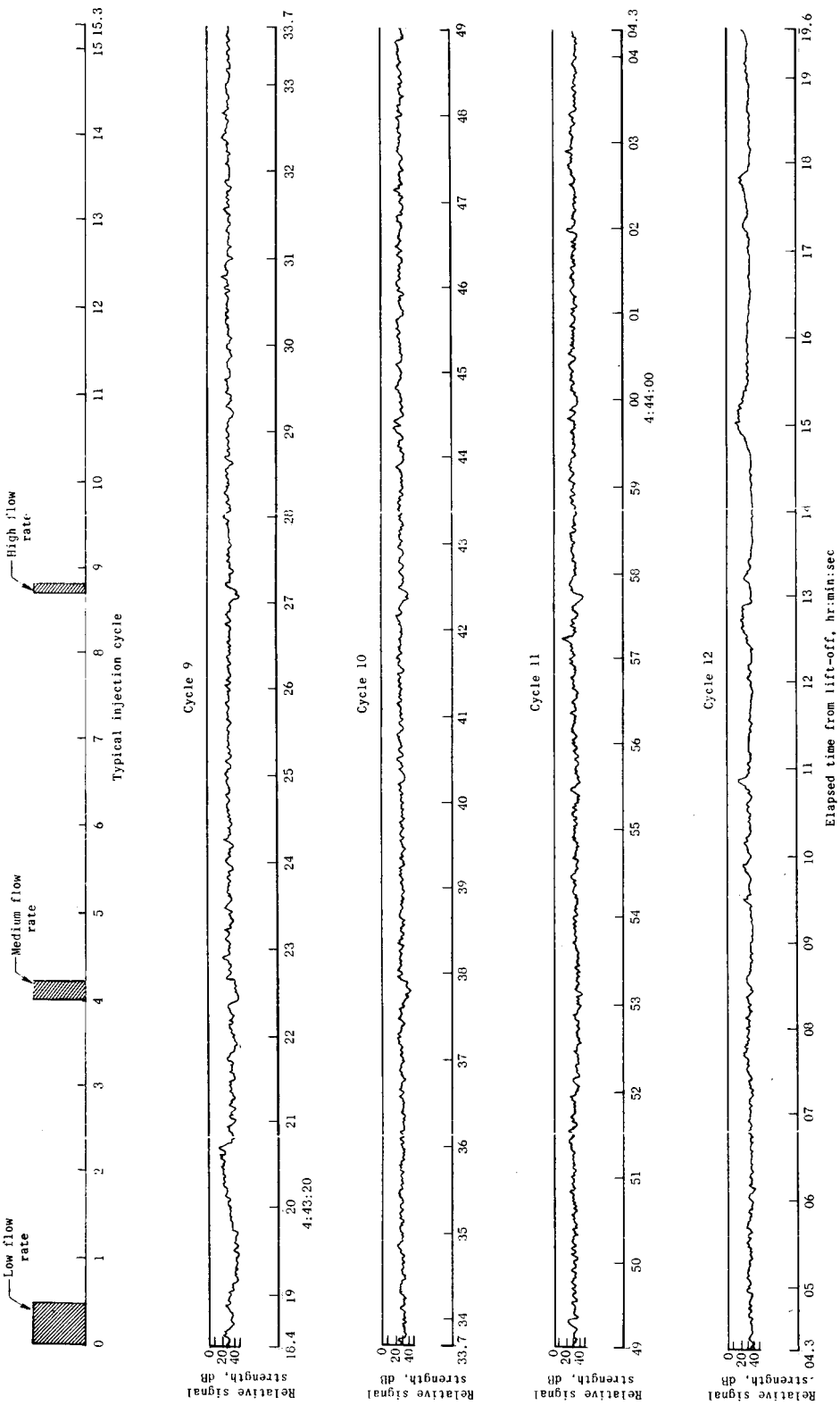


Figure 14.- Time history of C-band signal strength at Grand Bahama Island station.

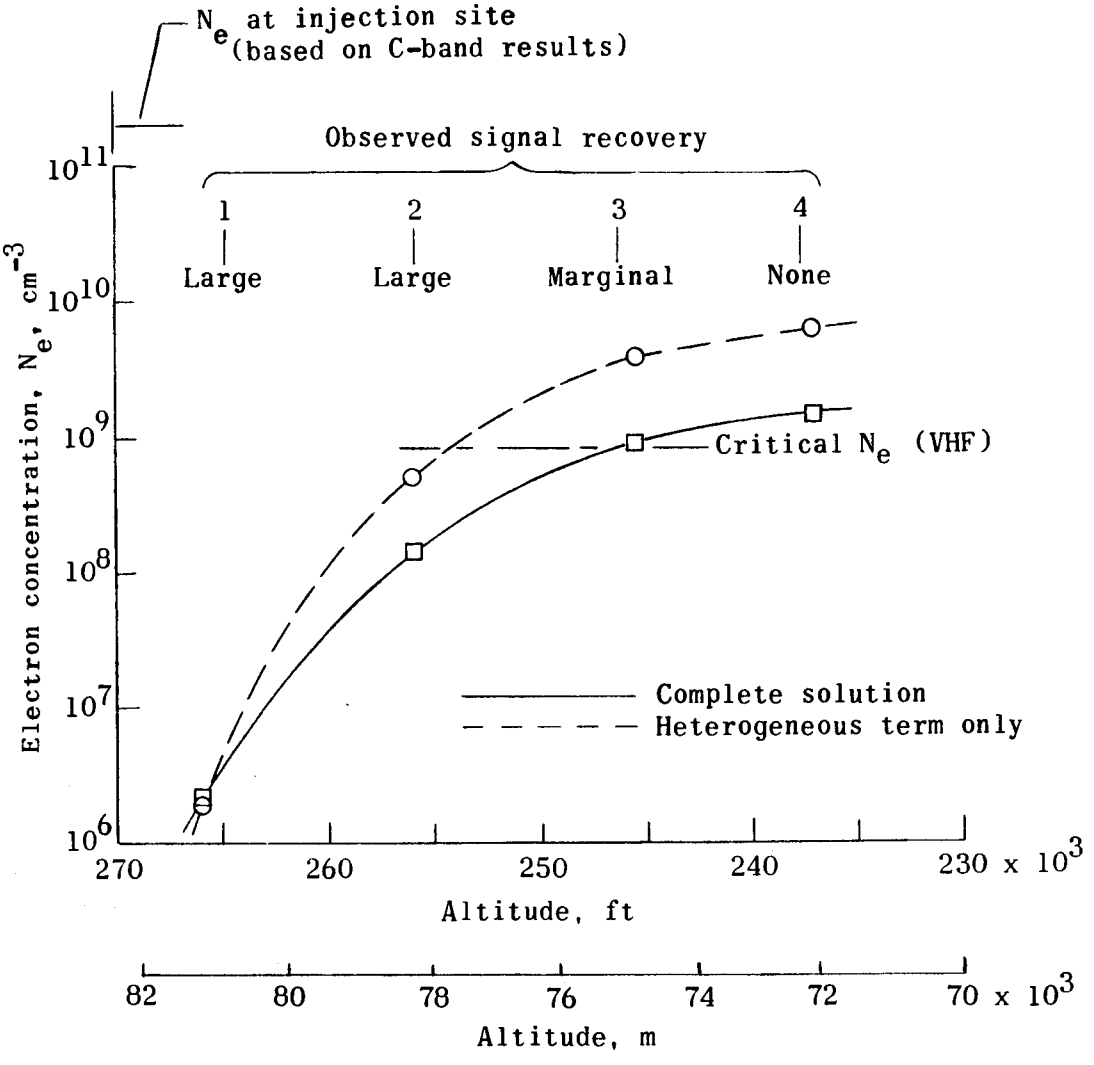


Figure 15.- Theoretical prediction of the effect of water injection on inviscid $N_e$ in the vicinity of the VHF antenna site.

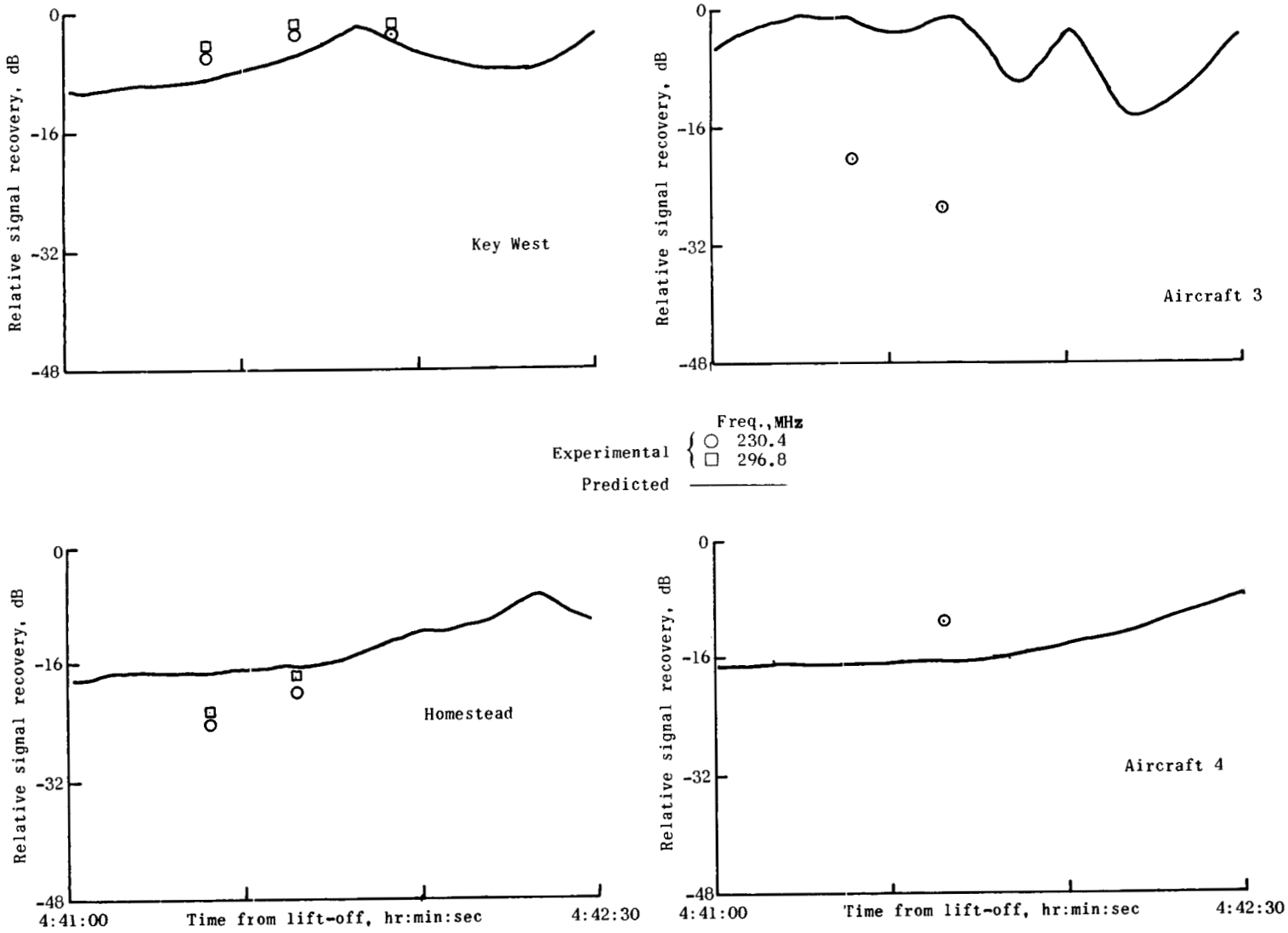


(a) Receiving stations south of flight path.

Figure 16.- Predicted and experimental VHF signal-recovery profiles.

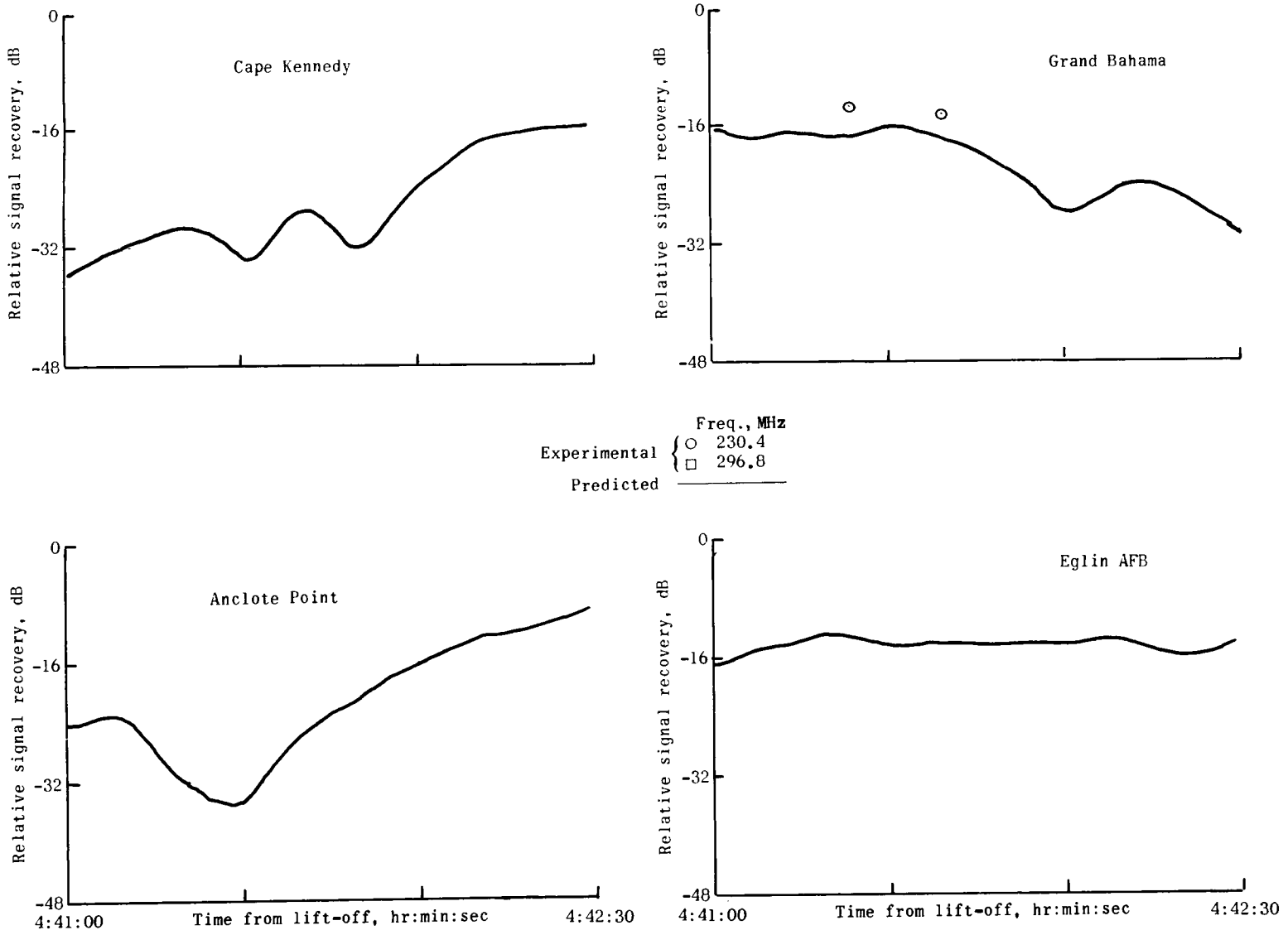


(b) Receiving stations north of flight path.

Figure 16.- Concluded.

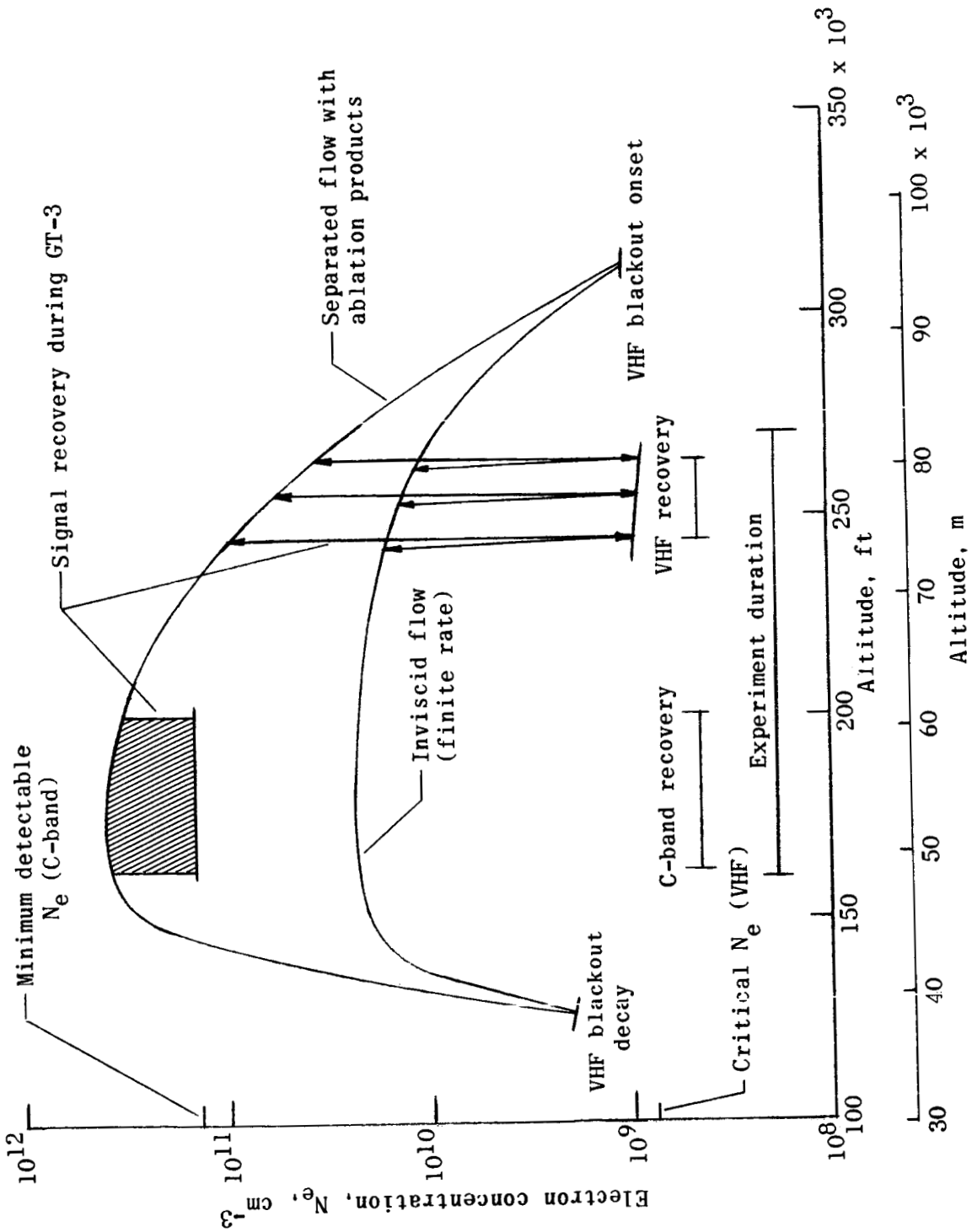


Figure 17.- Predicted free $N_e$ levels for the inviscid and separated-flow plasmas for the Gemini 3 reentry.

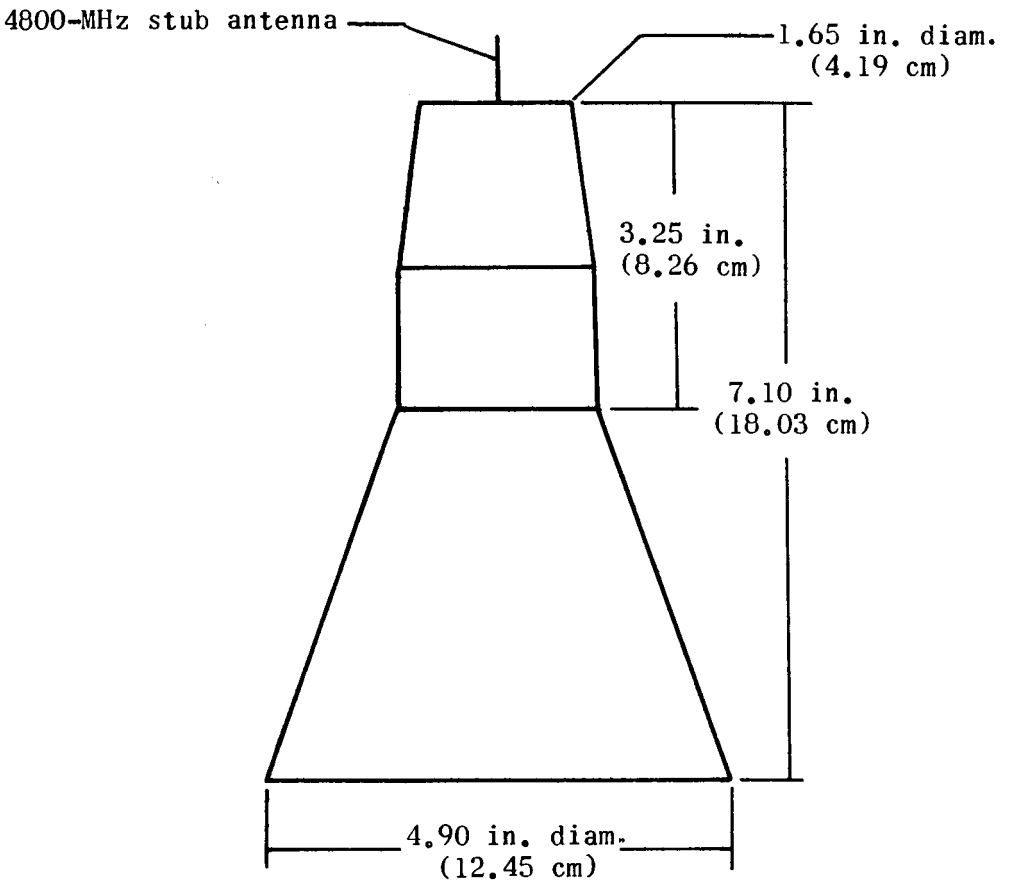


Figure 18.- The $\frac{1}{18}$-scale test model.

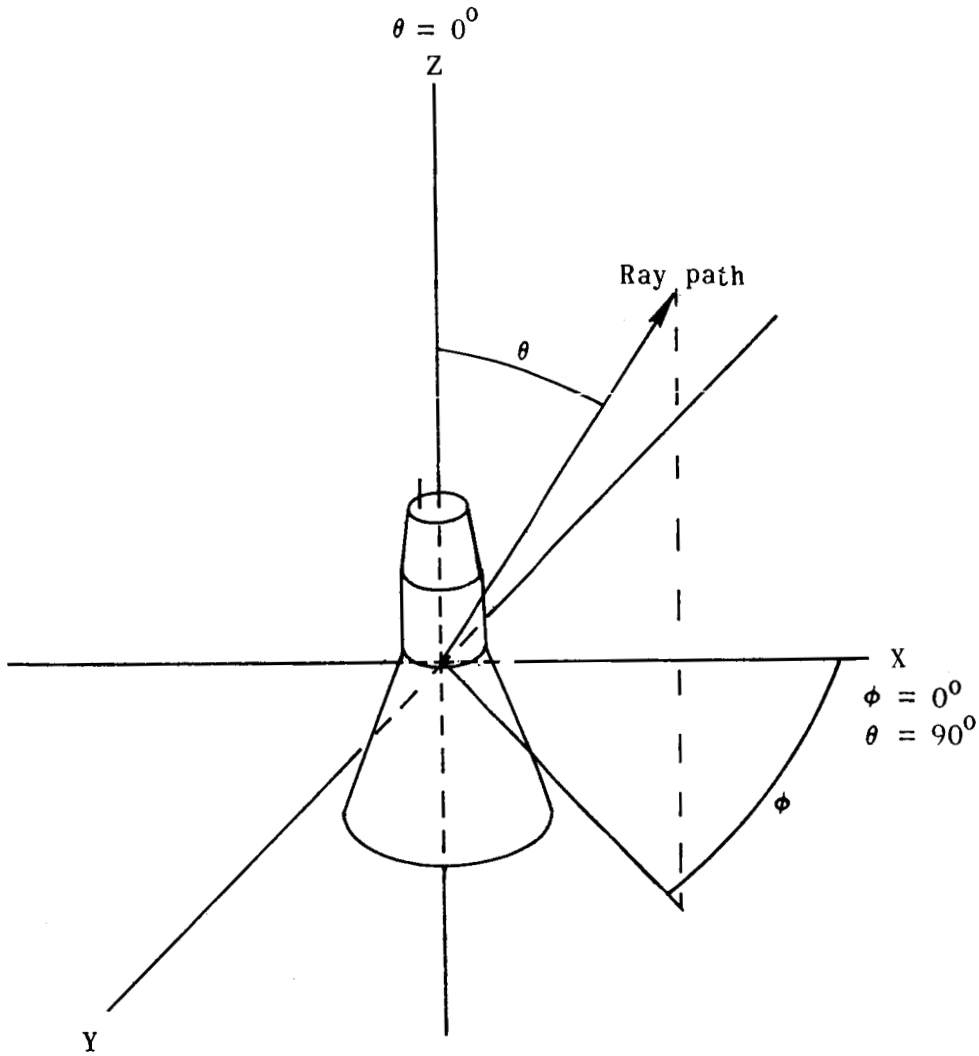


Figure 19.- Antenna coordinate system (left handed).

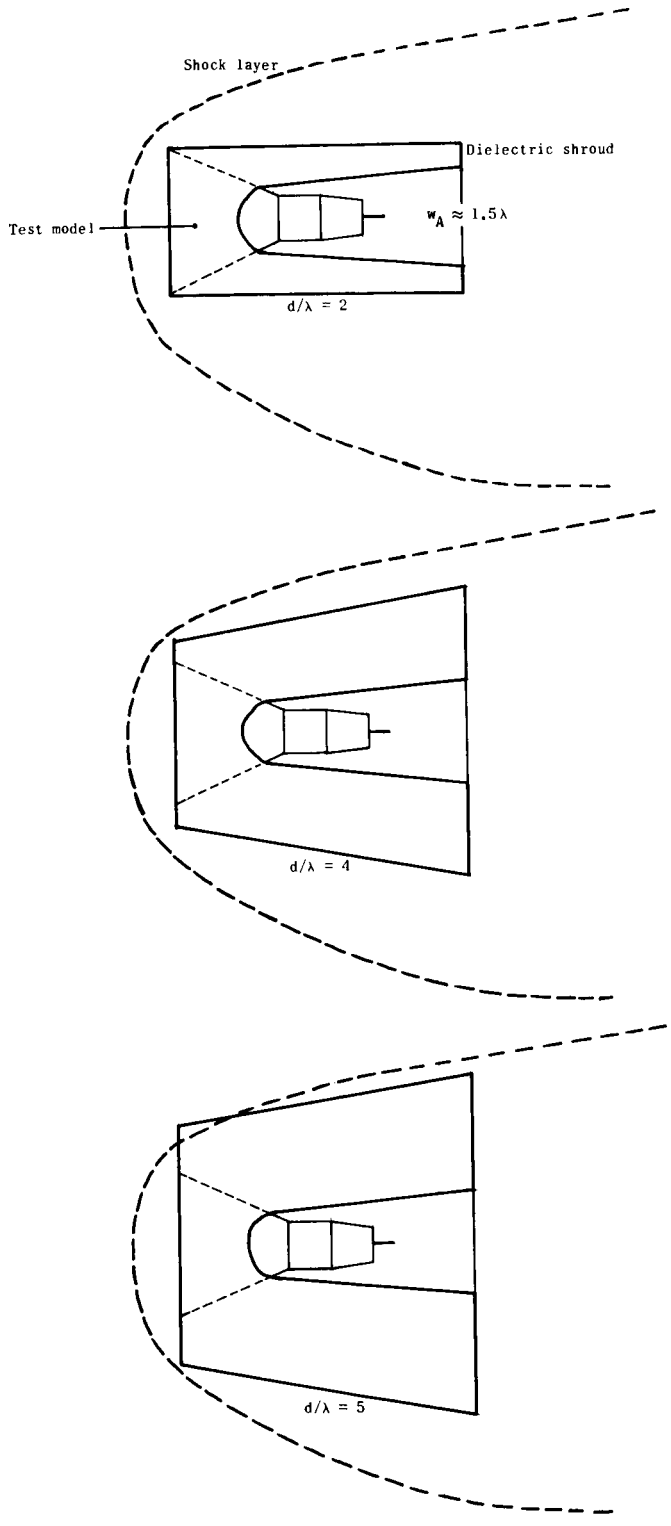


Figure 20.- Comparison of shroud configurations with typical Gemini flow field. (Shroud diameter d is measured at aft end of shroud.)

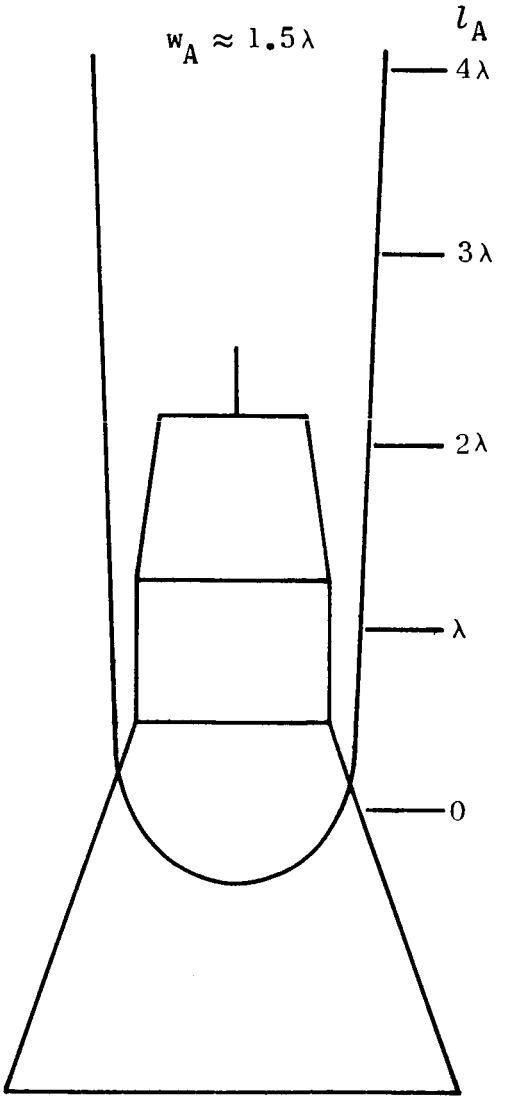


Figure 21.- Aperture length relative to antenna location.

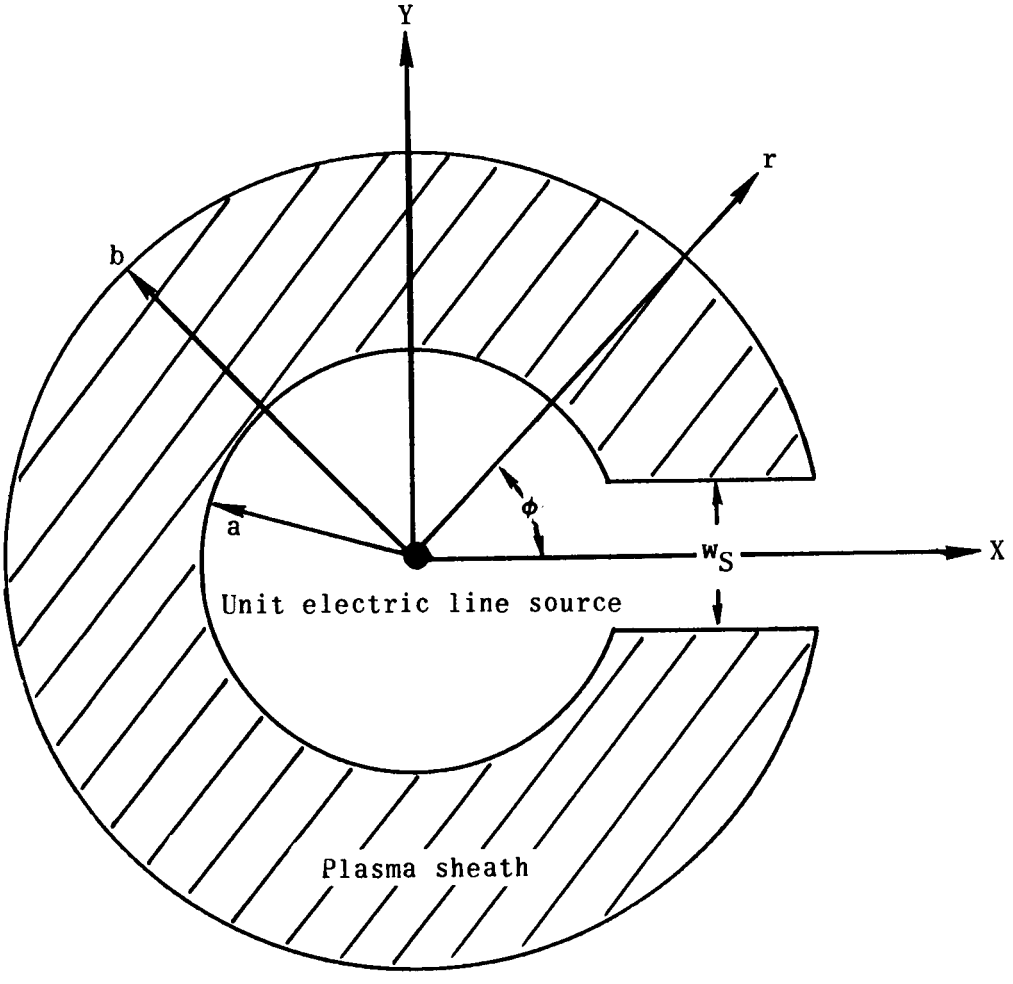


Figure 22.- Theoretical model of slotted plasma sheath. Sheath thickness t = b - a.

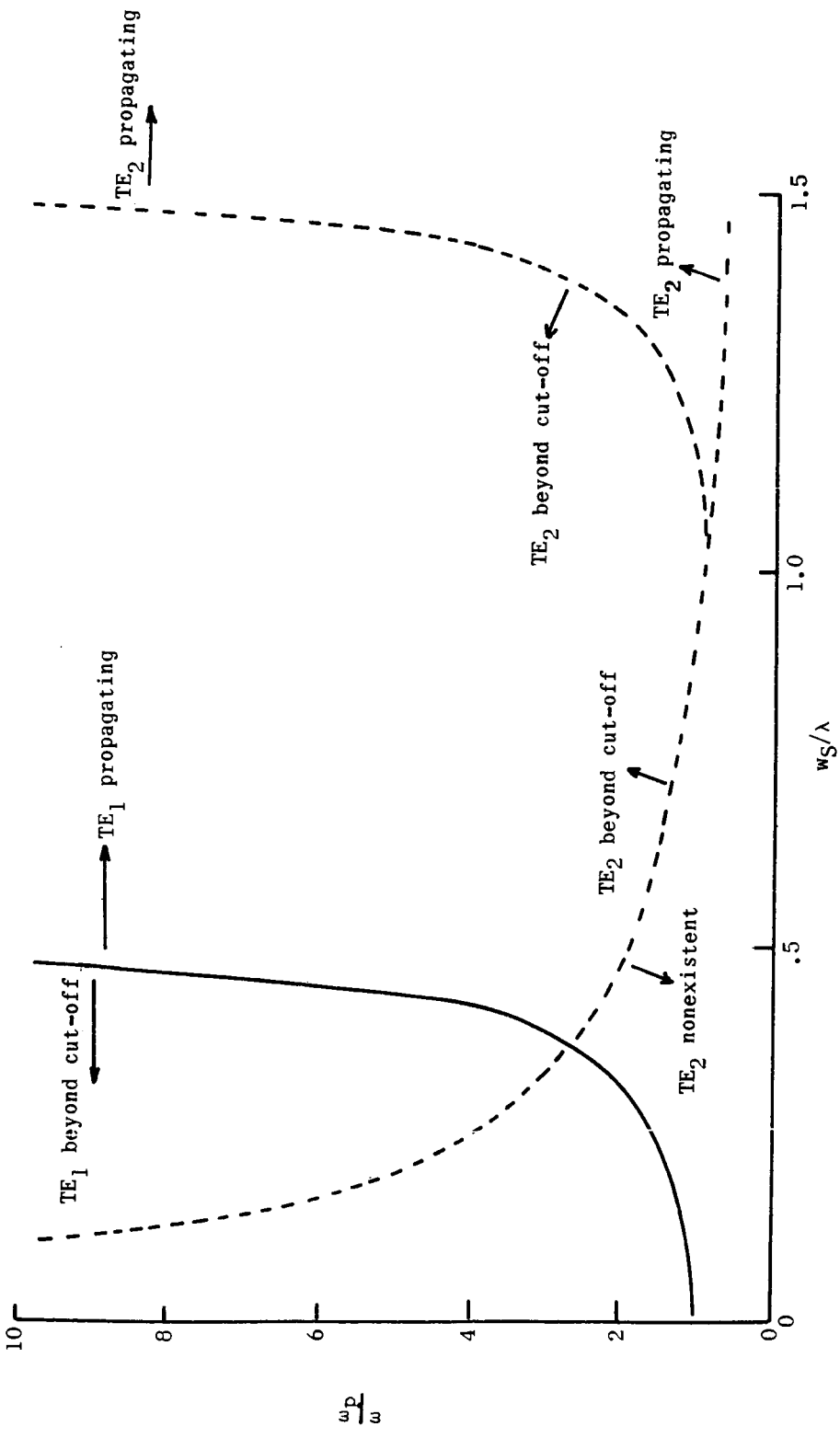


Figure 23.- Propagation and cut-off for two lowest order transverse electric modes.

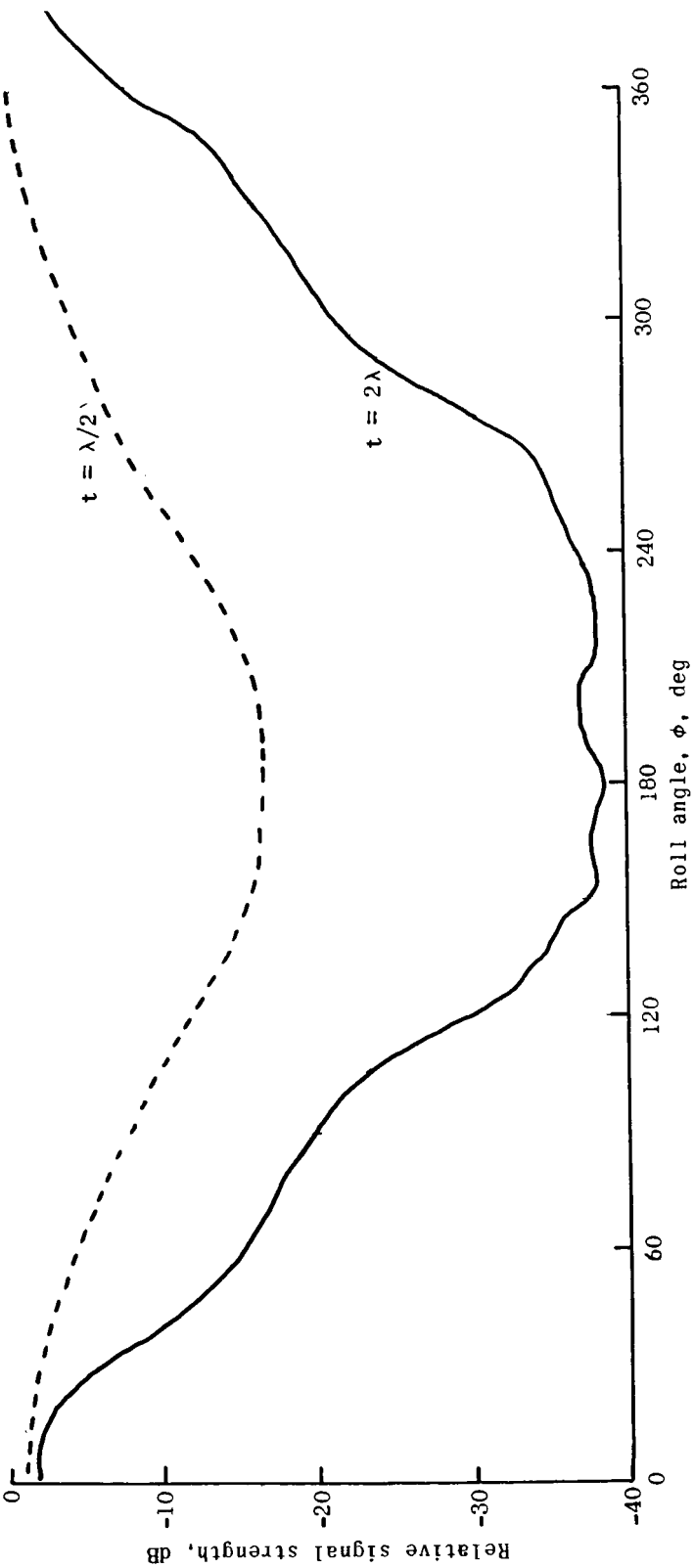


Figure 24.- Theoretical radiation patterns of antenna model. Slot width $w_S = \lambda/2$.

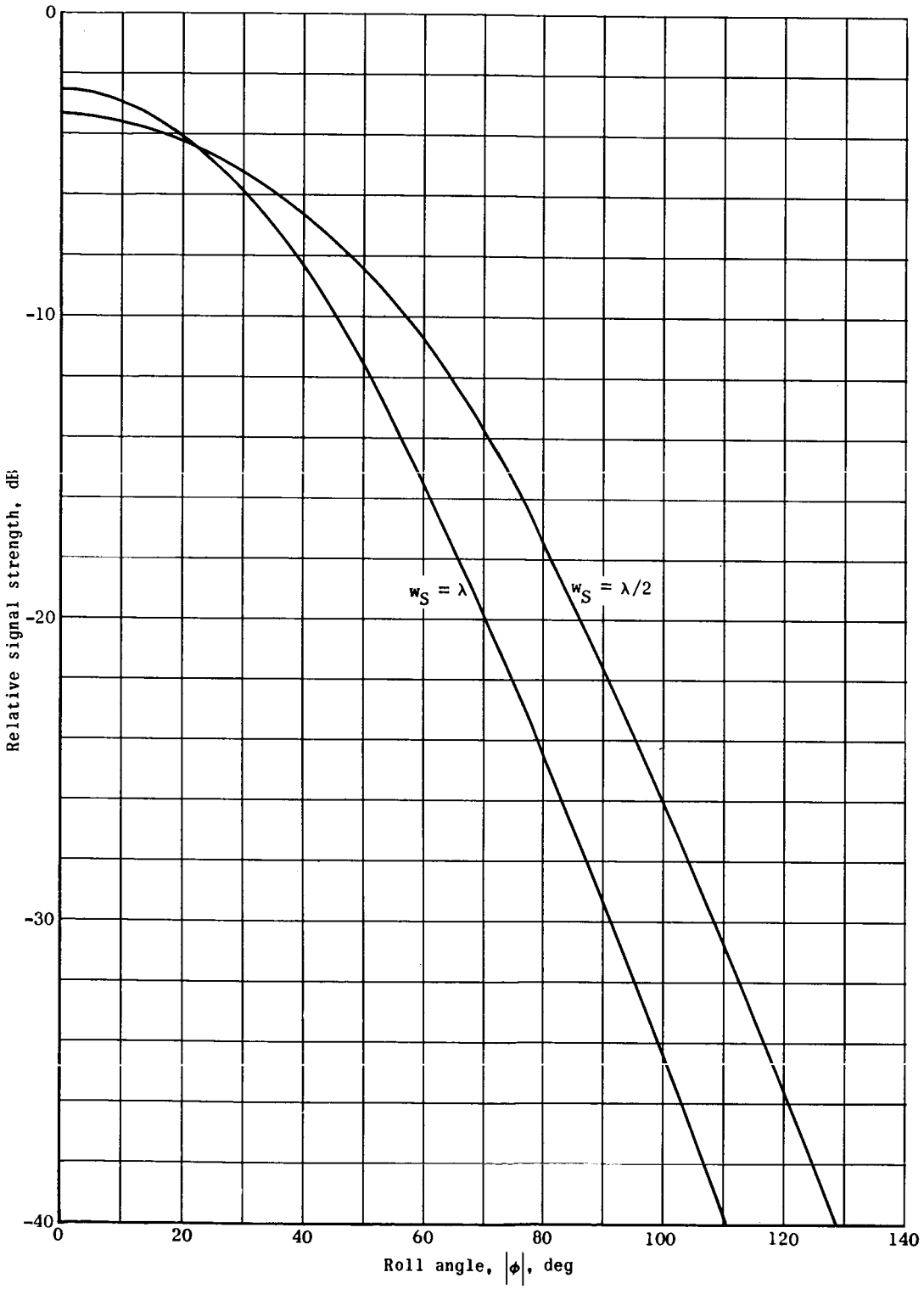


Figure 25.- Computed radiation field for slotted plasma sheath. Sheath thickness $t = 3\lambda$.

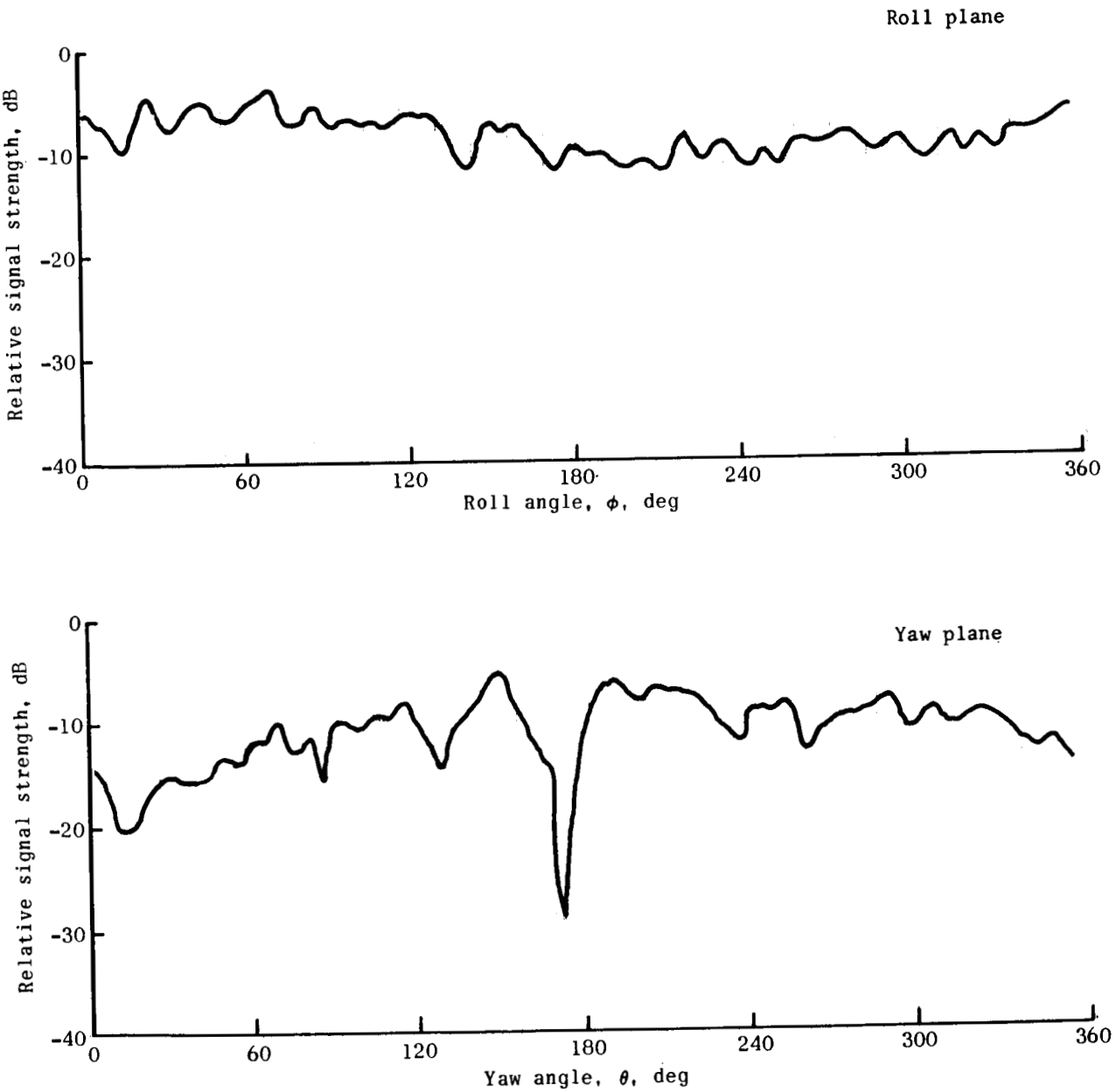


Figure 26.- Free-space pattern characteristics.

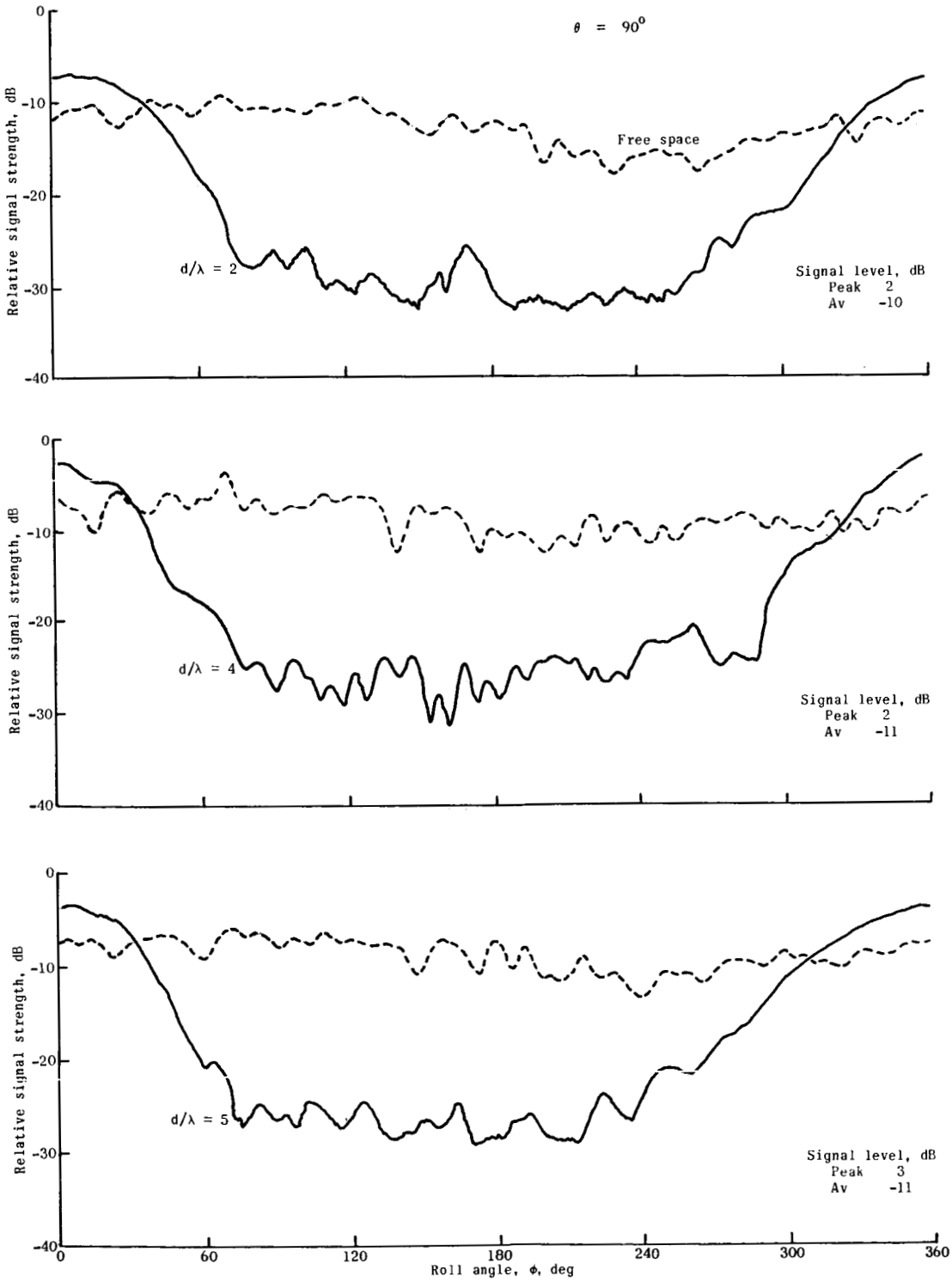


Figure 27.- Roll-plane signal strength as a function of sheath thickness. Aperture length $l_A = 3\lambda$.

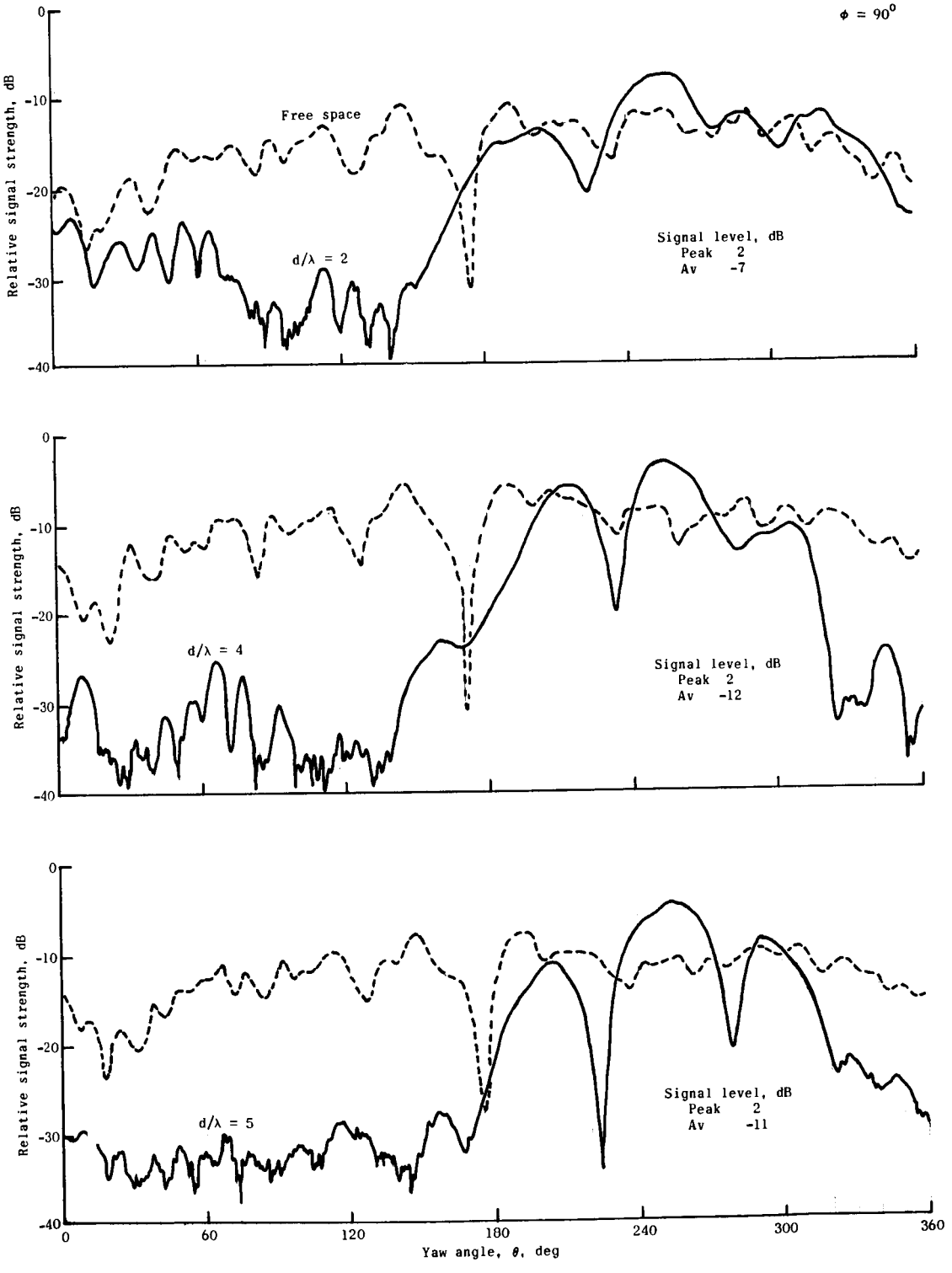


Figure 28.- Yaw-plane signal strength as a function of sheath thickness. Aperture length $l_A = 3\lambda$.

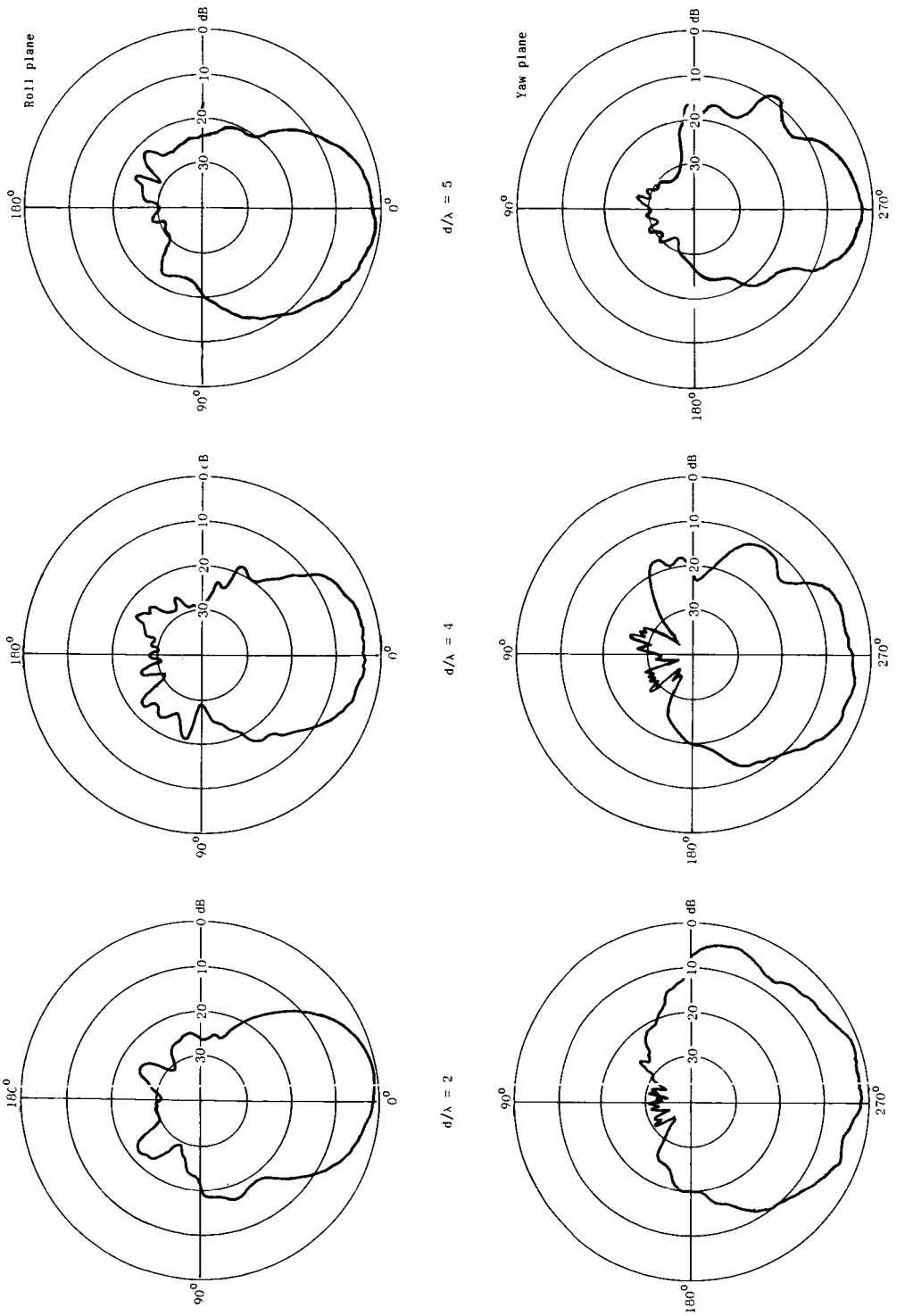


Figure 29.- Polar plots of signal strength as a function of sheath thickness. Aperture length $l_A = 4\lambda$.

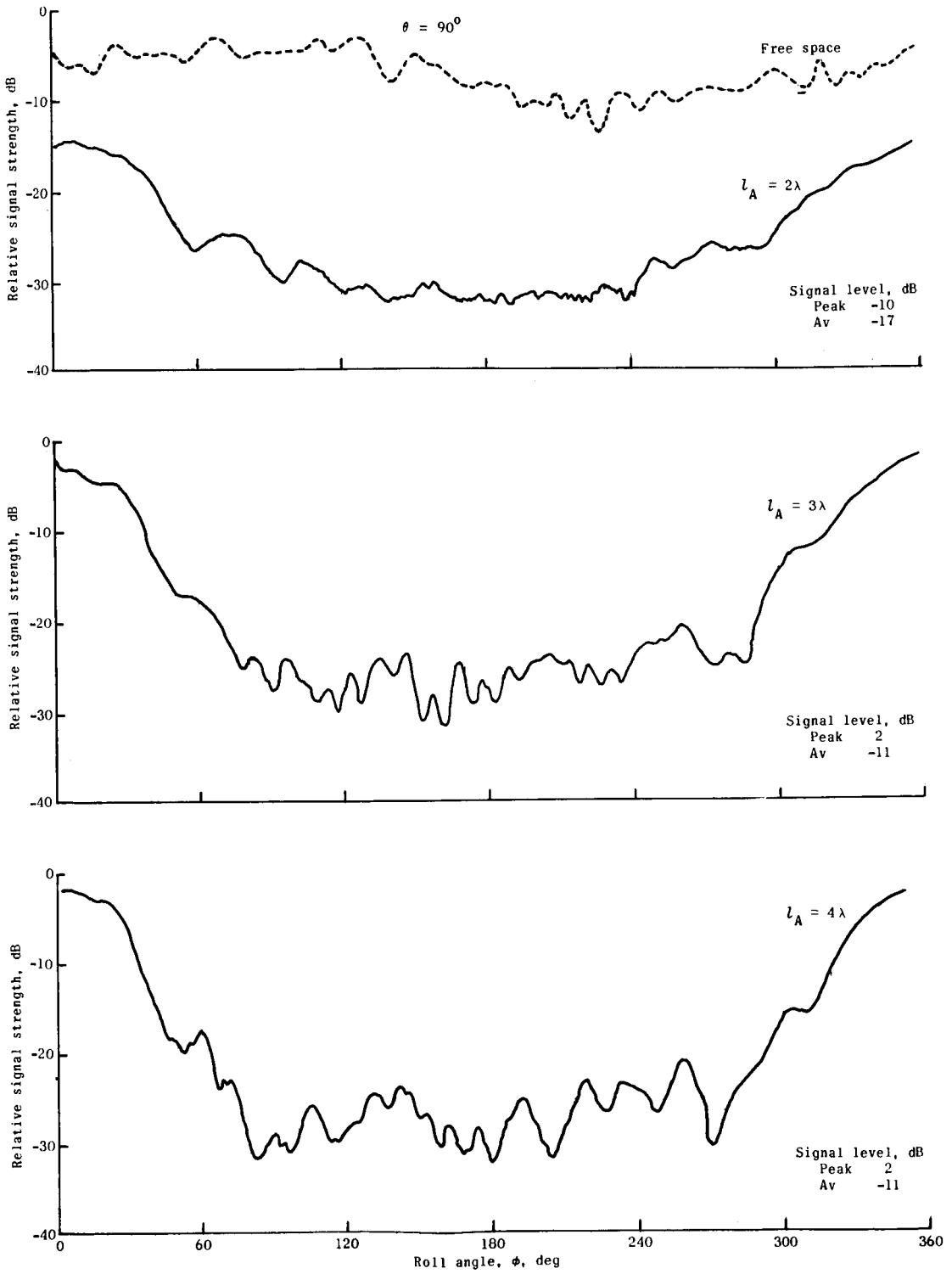


Figure 30.- Roll-plane signal strength as a function of aperture length. Sheath thickness t = 2λ.

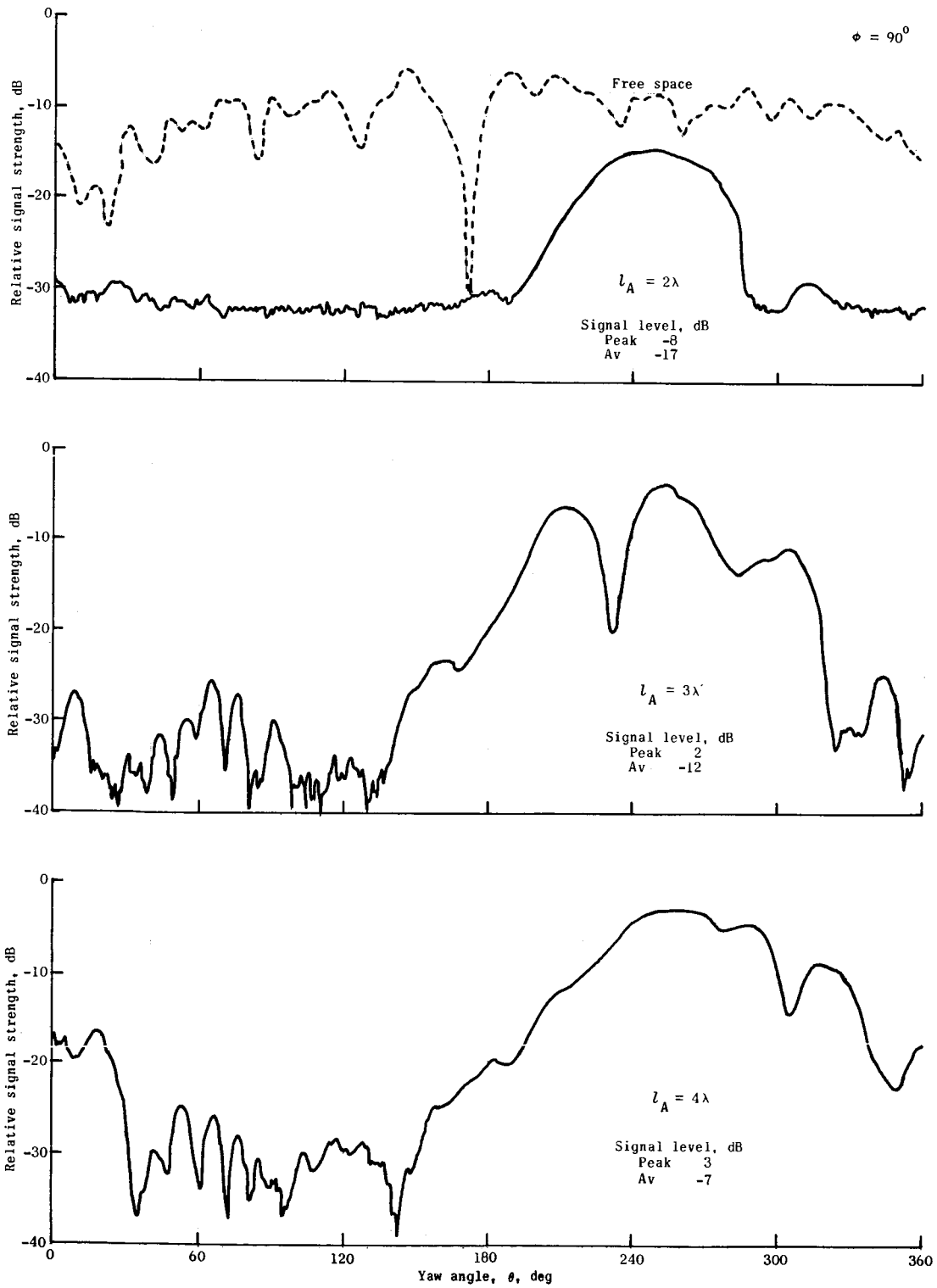


Figure 31.- Yaw-plane signal strength as a function of aperture length. Sheath thickness t = 2λ.

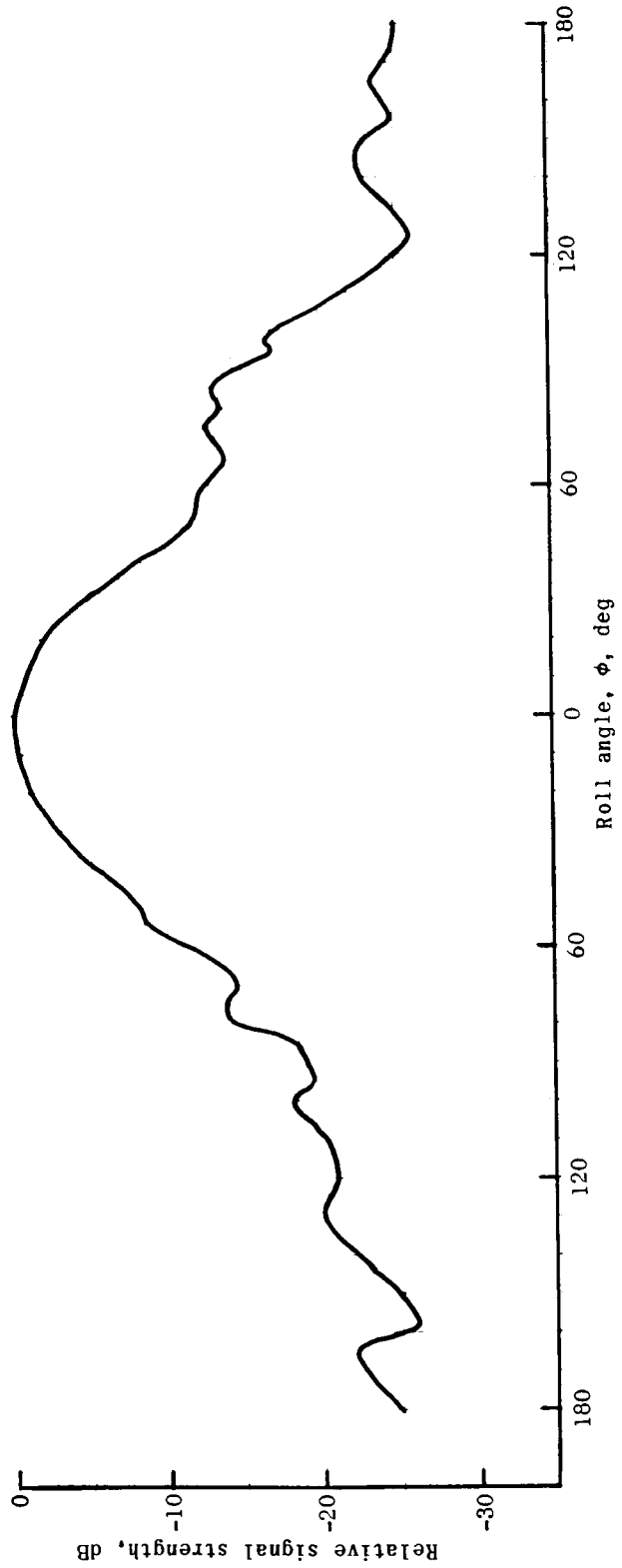


Figure 32.- Signal strength as a function of vehicle roll. $\theta = 90^{0}$.

*"The aeronautical and space activities of the United States shall be conducted so as to contribute . . . to the expansion of human knowledge of phenomena in the atmosphere and space. The Administration shall provide for the widest practicable and appropriate dissemination of information concerning its activities and the results thereof."*

—NATIONAL AERONAUTICS AND SPACE ACT OF 1958

# NASA SCIENTIFIC AND TECHNICAL PUBLICATIONS

**TECHNICAL REPORTS:** Scientific and technical information considered important, complete, and a lasting contribution to existing knowledge.

**TECHNICAL NOTES:** Information less broad in scope but nevertheless of importance as a contribution to existing knowledge.

**TECHNICAL MEMORANDUMS:** Information receiving limited distribution because of preliminary data, security classification, or other reasons.

**CONTRACTOR REPORTS:** Scientific and technical information generated under a NASA contract or grant and considered an important contribution to existing knowledge.

**TECHNICAL TRANSLATIONS:** Information published in a foreign language considered to merit NASA distribution in English.

**SPECIAL PUBLICATIONS:** Information derived from or of value to NASA activities. Publications include conference proceedings, monographs, data compilations, handbooks, sourcebooks, and special bibliographies.

**TECHNOLOGY UTILIZATION PUBLICATIONS:** Information on technology used by NASA that may be of particular interest in commercial and other non-aerospace applications. Publications include Tech Briefs, Technology Utilization Reports and Notes, and Technology Surveys.

*Details on the availability of these publications may be obtained from:*

SCIENTIFIC AND TECHNICAL INFORMATION DIVISION

NATIONAL AERONAUTICS AND SPACE ADMINISTRATION

Washington, D.C. 20546